Journal of Machine Learning Research 1 (2014) 1-34 Submitted 2/14; Published xx/14

Transduction on Directed Graphs via Absorbing Random Walks

Jaydeep De JAYDEEPD@BII.A-STAR.EDU.SG
*Bioinformatics Institute, A*STAR, Singapore*
School of Computer Engineering, Nanyang Technological University, Singapore

Xiaowei Zhang ZHANGXW@BII.A-STAR.EDU.SG
*Bioinformatics Institute, A*STAR, Singapore*

Li Cheng CHENGLI@BII.A-STAR.EDU.SG
*Bioinformatics Institute, A*STAR, Singapore*
School of Computing, National University of Singapore, Singapore

Editor: TBD

Abstract

In this paper we consider the problem of graph-based transductive classification, and we are particularly interested in the directed graph scenario which is a natural form for many real world applications. Different from existing research efforts that either only deal with undirected graphs or circumvent directionality by means of symmetrization, we propose a novel random walk approach on directed graphs using *absorbing* Markov chains, which can be regarded as maximizing the accumulated expected number of visits from the unlabeled transient states. Our algorithm is simple, easy to implement, and works with large-scale graphs. In particular, it is capable of preserving the graph structure even when the input graph is sparse and changes over time, as well as retaining weak signals presented in the directed edges. We present its intimate connections to a number of existing methods, including graph kernels, graph Laplacian based methods, and interestingly, spanning forest of graphs. Its computational complexity and the generalization error are also studied. Empirically our algorithm is systematically evaluated on a wide range of applications, where it has shown to perform competitively comparing to a suite of state-of-the-art methods.

Keywords: Random Walks on Directed Graphs, Transductive Learning, Absorbing Markov Chain, Transduction Generalization Error

1. Introduction

We focus on the following graph transduction problem: Given a directed graph with certain nodes labeled, make predictions on the rest unlabeled nodes by propagating the class labels following the underlining directed graph structure. Different from undirected graphs that delineate symmetric weight between adjacent nodes, in directed graphs, edge or link directions are well preserved in its weight matrix. This information is particularly useful in many real life applications that can be naturally characterized using directed graphs, including automated delineation of filamentary structures in images and videos (Hoover et al., 2000; Meijering et al., 2004; Staal et al., 2004; Turetken et al., 2013a,b), image classification (Cai et al., 2012) and clustering (Chen et al., 2010), network & link analysis in hyperlinks of webpages as well as citations of papers (McCallum et al., 2000; Macskassy and Provost,

2007; Wang et al., 2010; Fouss et al., 2012), among others. Moreover, the fast pace of big data production and storage, together with the scarcity of annotated labels, also create the need for algorithms capable of scaling up to make predictions on large-scale directed graphs with few known labels.

Since being introduced by Vapnik in the nineties, many research efforts have already been devoted to graph-based transduction or transductive learning, as can be found in the comprehensive reviews of (Chapelle et al., 2006; Zhu and Goldberg, 2009). Most of the existing literature work with undirected graphs. For example, the harmonic functions on Gaussian fields (Zhu et al., 2003), the local and global consistency of (Zhou et al., 2004) the quadratic criterion (Bengio et al., 2006), the commute time kernel (Fouss et al., 2012), the partially absorbing random walks (Wu et al., 2012), and the greedy max-cut (Wang et al., 2013). Among these methods, a few has been specifically dedicated to directed graphs, including in particular (Zhou et al., 2005; Cai et al., 2012). One major difficulty in learning with directed graphs lies in the asymmetric nature of the weight matrix introduced by these directed edges or links. This is often regarded as cumbersome when aligning with the key concepts developed for undirected graphs that are symmetric by nature, such as graph Laplacians. It thus leads to the widely adopted symmetrization trick in e.g. the construction of graph Laplacians (Zhou et al., 2005), or co-link similarity matrices (Wang et al., 2010). Unfortunately important information conveyed by edge directions are still lost. There have been a few methods for large-scale transduction such as (Gartner et al., 2005; Subramanya and Bilmes, 2011), which are however not ready to be used for directed graphs.

We propose a random walk on absorbing Markov chains approach to the problem of transductive learning on directed graphs, where the edge directions – the key aspect of directed graphs, are well preserved. Our algorithm is intuitive to understand, easy to implement, and by working with absorbing Markov chains (Kemeny and Snell, 1976), the sparse nature of the graph structure is also retained, which would be important in the context of predictions on large-scale directed graphs.

The most related work is that of (Zhou et al., 2005), which generalizes their earlier framework of regularized risk minimization on undirected graphs (Zhou et al., 2004) to directed graphs by discriminatively normalizing in-links and out-links, as well as adopting the directed graph Laplacian of (Chung, 2005). The method of (Zhou et al., 2005) involves symmetric matrices due to the construction of digraph Laplacian (Chung, 2005), where the symmetrization trick is utilized. In contrast, we directly work with asymmetric matrices, which is the key in preserving edge directions. In addition, the construction in (Zhou et al., 2005) relies on an irreducible Markov chain, which however only apply to *strongly connected* directed graphs, that is, there is a directed path from any node to any other node of the graph. Since in practice the directed graphs are usually not necessarily strongly connected, a teleporting random walk trick (e.g (Page et al., 1998)) is adopted by inserting bi-directional edges between all node pairs with an equal weight. The resulting method thus works only with non-sparse matrices, instead our algorithm is able to preserve sparse graph structures and edge directional information of the input. Besides, our algorithm is able to efficiently work with large-scale graphs that might be too big to be considered by (Zhou et al., 2005). More recently, the family of partially absorbing random walks (PARW) is proposed in (Wu et al., 2012), which can be formulated as a special case of the absorbing Markov chains

considered in our approach. Note absorbing random walks have been considered by Zhu et al. (2007) for an entirely different problem in natural language processing.

The main contributions of this work are four folds. (1) A novel random walk on *absorbing* Markov chain approach is proposed to the problems of transductive classification on directed graphs. (2) An efficient algorithm is provided that exploits the inherent sparse graph structure, while it also maintains and directly utilizes edge directional information. In addition, an optimal one-step increment/decrement update (aka online update) is introduced, which is handy in scenarios where local changes are made to graphs over time, or prediction are made on out-of-sample instances. The proposed algorithm also bears interesting connections to existing works including undirected graph Laplacian, diffusion graph kernels, spanning forest of graphs, graph-based proximity measure, among others. (3) We present several interesting properties of the E matrix, a central element in our approach. Many of them are new to our best knowledge. (4) We conduct theoretical analysis on its generalization error, as well as extensive and systematic empirical simulations on various applications to examine the characteristics of the proposed algorithm and its performance with respect to existing state-of-the-art methods.

2. Our Approach: Random Walks on Directed Graphs

Problem Set-up Let $G = (\mathcal{V}, \mathcal{E}, W)$ denote a directed graph or digraph, where $\mathcal{V} = \{v_1, v_2, \dots v_n\}$ is the set of nodes, $\mathcal{E}$ is the set of directed edges each connecting two adjacent nodes, and $W = [w_{ij}] \in \mathbb{R}^{n \times n}$ is the asymmetric non-negative matrix with $w_{ij} \geq 0$ denoting the weight associated with the directed edge from v_i to v_j. The in-degree of each node v_j is computed as $d_j^- = \sum_{i=1}^n w_{ij}$, and define in-degree matrix $D = \text{diag}(d_1^-, \cdots, d_n^-)$. A column stochastic transition probability matrix, $P = [p_{ij}]$, can be constructed as $p_{ij} = \frac{w_{ij}}{d_j^-}$, or equivalently as $P = WD^{-1}$. Note *loops*, *self-loops*, and *bi-directional* edges (i.e. two edges between adjacent nodes) are allowed, as e.g. illustrated in Figure 1(a). An important remark is that random walks on an undirected graph can be regarded as a special case in our context, since in its weight matrix W, the symmetric pair w_{ij} and w_{ji} correspond to bi-directional edges with the same weights – which can be characterized by a reversible Markov chain. In this paper, we focus on a transductive inference scenario where labels from the set of few labeled nodes $\mathcal{V}_l$ are to be propagated to the rest nodes, namely the set of unlabeled nodes $\mathcal{V}_u$, with $\mathcal{V} = \mathcal{V}_l \cup \mathcal{V}_u$. The labels here could be binary or multiclass. To simplified the notation we assume $\mathcal{V}_l$ contains the first l nodes, $\mathcal{V}_l = \{v_1, \dots, v_l\}$. To accommodate label information, define a label matrix Y of size $n \times K$ (assuming there are K class labels available), with each entry Y_{ik} containing 1 provided the node i belongs to $\mathcal{V}_l$ and is labeled with class k, and 0 otherwise. Besides, define the ground-truth label vector $\mathbf{y}$, a vector of length n including two disjoint parts $\mathbf{y}_l$ and $\mathbf{y}_u$: $\mathbf{y}_l$ is the input label vector of length l over the set of labeled nodes, with each entry y_i for the input class assignment of node $v_i \in \mathcal{V}_l$; $\mathbf{y}_u$ is the hold-out ground-truth label for the unlabeled nodes, i.e. a vector of length $n - l$. Similarly, define the initial label vector $\hat{\mathbf{y}}$ containing also two parts, $\hat{\mathbf{y}}_l := \mathbf{y}_l$ and $\hat{\mathbf{y}}_u = \mathbf{0}$, where $\mathbf{0}$ is an all zero vector of length $n - l$. Define the prediction vector $\mathbf{y}^*$ with also two parts $\mathbf{y}_l^* := \mathbf{y}_l$, as well as $\mathbf{y}_u^*$ of length $n - l$, containing the prediction results, where each y_i^* denotes the predicted class assignment for a node $v_i \in \mathcal{V}_u$.

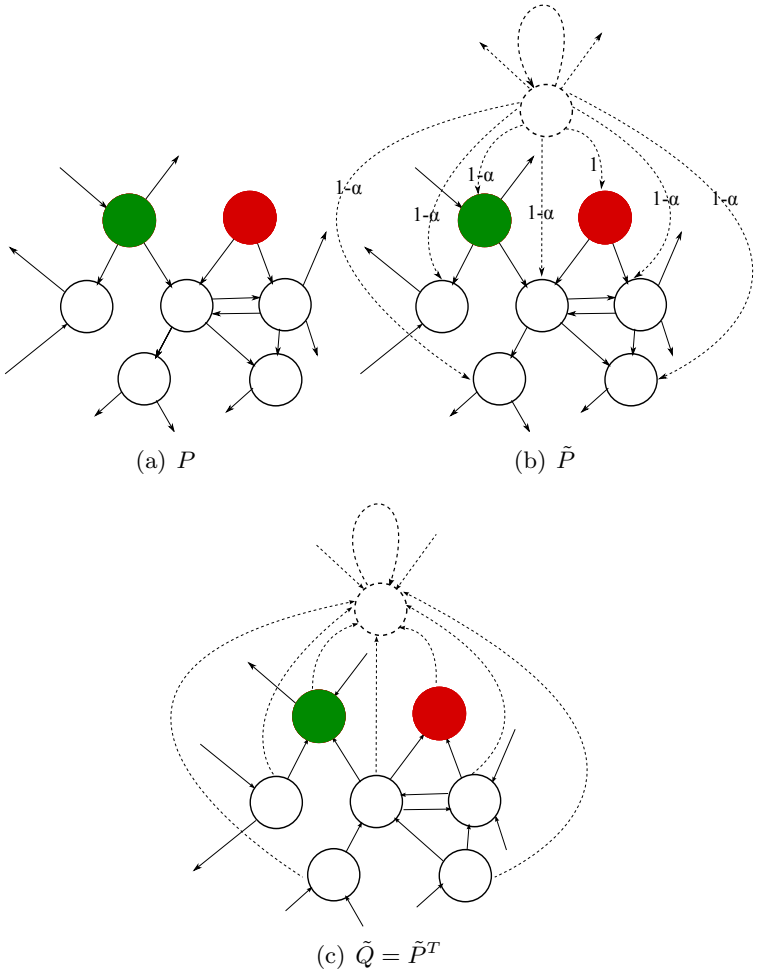

(a) P (b) $\tilde{P}$

(c) $\tilde{Q} = \tilde{P}^T$

Figure 1: (a) An illustrative example of a weighted digraph-based transduction setting: Two different class labels are to be propagated from the labeled nodes (the green and the red nodes, each for one class) to the rest nodes following the graph structure. Here only a subset of the graph nodes and edges are displayed. Quantities such as W and P can be computed accordingly. (b) As some nodes might have zero in-degree (i.e. source nodes), a new node is further added with directed edges to every nodes including itself, which gives $\tilde{P}$. According to the $\mathbf{c}$ vector, the edges toward those previous source nodes are weighted by 1, and the rest are $1 - \alpha$. (c) Its transpose, $\tilde{Q}$, corresponds to the same graph but with edge directions being reversed. This facilitates the evaluation of affinity scores flowing from unlabeled nodes (e.g. leaf nodes) to the labeled nodes (e.g. source nodes).

Our Absorbing Markov Chain and its Fundamental Matrix There however exists an issue: the graph often contains source nodes (i.e. nodes with $d_j^- = 0$ [1]), for which the corresponding columns in P are zero vectors – then P is not stochastic anymore. Inspired by the PageRank method used in Google search engine (Page et al., 1998), we consider an augmented graph to ameliorate this situation: One extra node v_{n+1} is introduced that is

1. Usually source nodes are within $\mathcal{V}_l$, i.e. they are labeled nodes.

further connected to each of the source nodes $\mathcal{V}_l$ with a equal weight of 1 and connected to the rest nodes with a equal weight of $(1-\alpha)$ where $\alpha \in (0,1)$. A self-connecting edge $e = (v_{n+1}, v_{n+1})$ with a transition probability 1 is further imposed on this new node v_{n+1}, to save itself from being another source node. This leads to a digraph as displayed in Figure 1(b), which also corresponds to an augmented column-stochastic transition probability matrix

$$\tilde{P} = \left(\begin{array}{c|c} \alpha P & 0 \\ \hline \mathbf{c} & 1 \end{array}\right) \in \mathbb{R}^{(n+1)\times(n+1)},$$

where $\mathbf{c} \in \mathbb{R}^{1\times n}$ is a vector with the elements corresponding to source nodes being 1 and the rest elements being $1-\alpha$.

Let us pause for a moment and recall that in our context, labels of the source nodes (if there are any) are usually known and are to be propagated to the rest nodes including the leaf nodes. Edges of the input graph however flows from source to leaf nodes, as exemplified in Figure 1(b) for $\tilde{P}$. It is more informative to *reverse* all the edge directions, to compute instead the affinity of each unlabeled node toward the labeled nodes (where many are source nodes). As presented in Figure 1(c), algebraically this corresponds to the matrix *transpose*, $\tilde{Q} := \tilde{P}^T$. Surprisingly, now this row-stochastic transition probability matrix

$$\tilde{Q} \;=\; \left(\begin{array}{c|c} \alpha P^T & \mathbf{c}^T \\ \hline 0 & 1 \end{array}\right) = [\tilde{q}_{ij}] \tag{1}$$

defines an *absorbing Markov chain* on the augmented digraph, $\tilde{G}$. Considering random walks in the Markov chain theory (Kemeny and Snell, 1976), each node v_i of the digraph is equivalent to a Markov chain state s_i, and collectively, the set of nodes naturally identifies a set of states $S = \{s_1, s_2, \ldots, s_{n+1}\}$ in the Markov chain induced by the graph $\tilde{G}$ of $n+1$ nodes. In what follows node v and state s are sometimes used interchangeably. In addition, s_{n+1} is the only absorbing state, while $S_t = \{s_1, s_2, \ldots, s_n\}$ denotes the set of transient or non-absorbing states connecting to s_{n+1} by at least one path. Here each entry $\tilde{q}_{ij}$ with $s_i, s_j \in S_t$ denotes the transition probability from state s_i to state s_j. It is also known that within a finite number of steps, a particle in state s_i moving randomly by $\tilde{Q}$ will be absorbed into s_{n+1} with probability 1.

Let us inspect further the upper left block of the matrix $\tilde{Q}$ in (1), denote $Q = \alpha P^T = [q_{ij}]$, and I an identity matrix, both of size $n \times n$. From Markov chain theory (Kemeny and Snell, 1976) we know every element of $Q^t = \underbrace{Q \ldots Q}_{t}$ denotes the probability of a particle starting from s_i to visit s_j in t steps. The expected number of visits from s_i to s_j ($s_i \to s_j$) in t steps is $e_t(s_i \to s_j) = \sum_{k=0}^{t} q_{ij}^{(k)}$, or in its matrix form

$$E_t = I + Q + Q^2 + \ldots + Q^t. \tag{2}$$

Proposition 1 *The fundamental matrix of the absorbing Markov chain $\tilde{Q}$ is*

$$E = (I - \alpha P^T)^{-1} = [e_{ij}]. \tag{3}$$

The detailed proof is described in Appendix A. In what follows, we present a transductive learning algorithm based on the fundamental matrix of the above absorbing Markov chain $\tilde{Q}$.

Our Algorithm Maximizes the Accumulated Expected Number of Visits An important fact (Kemeny and Snell, 1976) about the fundamental matrix E of our Markov chain $\tilde{Q}$ is that its (i, j)-th entry e_{ij} provides the *expected number of times* a particle from a transient state s_i visits the transient state s_j. This provides a notion of affinity from state i to j. The intuition is, if a state j is close to the initial state i in terms of graph structure, it will be visited by the particle more often than if it is far away from initial state (We visit our close relatives more often than our distant ones). Now define the affinity matrix as

$$A = EY = (I - \alpha P^T)^{-1} Y. \tag{4}$$

It is a matrix of size $n \times K$, with each entry a_{ik} being associated with an affinity score of state i belonging to class k. In other words, it is the accumulated expected number of visits from state v_i to those states in $\mathcal{V}_l$ that are labeled with class k. Here $\alpha \in (0, 1)$ acts as a parameter which controls how long the random walker stays among the transient states before it gets absorbed. If α is closer to 1 then the random walker stays for a longer period of time before getting absorbed, and vice versa. Empirically it is observed that our approach is insensitive to varying α values to anything between .01 and .99. We set $\alpha = 0.1$ throughout the experiments. To infer $\mathbf{y}_u^*$ of the unlabeled states $\mathcal{V}_u$, our algorithm predicts each entry's class assignment by identifying a label with the largest affinity score, namely

$$\mathrm{y}_i^* = \arg\max_k a_{ik}, \qquad \forall v_i \in \mathcal{V}_u. \tag{5}$$

Multi-label Classification With slight modification our approach is also able to work with multi-label classification. That is, starting with a few nodes of the input graph being labeled, to predict multiple target labels for each of the rest nodes. Instead of Y, we consider a matrix $\tilde{Y}$ of size $n \times \tilde{K}$ for the input label matrix. Here, each column of $\tilde{Y}$ is for one of the $\tilde{K}$ labels, and each entry contains $\tilde{Y}_{ik} = 1$ if the i-th instance is positive for label k, -1 if it is a negative instance, or 0 if it is unlabeled. Instead of $\mathbf{y}^*$, define $\tilde{Y}^*$ the prediction matrix of size $n \times \tilde{K}$. To infer the row vectors $\tilde{Y}^*_{u:}$ of the unlabeled states $\mathcal{V}_u$ from the incurred affinity matrix $A = [a_{ik}]$, we replace (5) with the following one: $\forall v_i \in \mathcal{V}_u, k \in \{1, \cdots, K\}$, $\tilde{y}^*_{ik} = 1$ if $a_{ik} > 0$, and $\tilde{y}^*_{ik} = -1$ otherwise. In other words, a particular entry is assigned positive, if its accumulative expected number of visits to positively labeled instances is more than that to those negative ones, and vice versa. The same procedure can be carried on over all labels.

Algorithm 1 Transduction by Random Walks on Directed Graphs

Input: A digraph $G = (\mathcal{V}, \mathcal{E}, W)$, label information Y, $\mathbf{y}_l$, and $\alpha \in (0, 1)$.
Output: $\mathbf{y}_u^*$
Compute the in-degree matrix D.
Compute the transition probability matrix $P = WD^{-1}$.
Compute the affinity matrix A by (4).
Produce prediction $\mathbf{y}_u^*$. The i-th entry is computed by (5), for an unlabeled node $v_i \in \mathcal{V}_u$.

One-step Increment/Decrement Update (aka Online Update) In a dynamic graph setting, over the time its graph weights or even structure might subject to changes, being

either inserting or deleting edges or nodes of the graph, or merely adjustments of the edge weights. Note the node insertion case corresponds to the out-of-sample instance scenario. These operations can all be accomplished by one-step increment/decrement edge update. In what follow we present a simple $O(n)$ procedure to perform such update in our context. Consider G (or G') being a digraph (its updated digraph) with transient submatrix $Q = \alpha P^T$ (Q'), and fundamental matrix E (E'), respectively. Our aim is to efficiently update E in the following three cases: (1) Delete an edge or decrease an edge weight, $\Delta q_{ij} < 0$; (2) Add an edge or increase an edge weight, $\Delta q_{ij} > 0$, and $\Delta q_{ij} e_{ji} \neq 1$; (3) Add a new node with its edges. Furthermore, the matrix Q has the property that the summation of each row equals either α or 0. In this case, a change of weight entry q_{ij} will lead to changes in the entire i-th row of Q. Fortunately, as described in Proposition 2 below, the cases described above can all be addressed, once we establish a mean to update E' by Proposition 2(i) focusing on the change of only a single entry q_{ij} between Q and Q':

Proposition 2 *(i) Suppose for an arbitrary entry q_{ij}, the amount of change, Δq_{ij}, satisfies $|\Delta q_{ij}| \leq q_{ij}$ if $\Delta q_{ij} < 0$, and $\Delta q_{ij} e_{ji} \neq 1$ otherwise. The incurred amount of change in E is*

$$\Delta E := E' - E = \frac{\Delta q_{ij}}{1 - \Delta q_{ij}\, e_{ji}} E_{:i}\, E_{j:} \tag{6}$$

where $E_{:i}$ and $E_{:j}$ denote the i-th column and j-th row of E, respectively.

(ii) Consider the changes in the entire i-th row of Q, and assume the amount of change in each entry satisfies the condition described above. To update matrix E, we can either apply (6) n times with each time dealing with one entry change, or equivalently apply the following result:

$$E' = E + \frac{E_{:i}(\Delta Q_{i:}\, E)}{1 - \Delta Q_{i:}\, E_{:i}}, \tag{7}$$

where $\Delta Q_{i:}$ denotes the amount of change in the i-th row of Q.

(iii) Suppose a new node is added to the graph such that the matrix Q becomes $Q' = \begin{bmatrix} Q & u \\ v^T & q \end{bmatrix}$, then the new fundamental matrix E' is given by

$$E' = \begin{bmatrix} E + \gamma(Eu)(v^T E) & \gamma(Eu) \\ \gamma(v^T E) & \gamma \end{bmatrix}, \tag{8}$$

where $\gamma = \frac{1}{(1-q) - v^T E u}$.

The proof is detailed in Appendix A. Notice the imposed condition of $\Delta q_{ij} e_{ji} \neq 1$ in (i) for adding an edge is to guarantee that E is well-defined. Empirically online updates are shown to produce the same results as the batch update counterpart (i.e. our normal algorithm), with negligible entry-wise difference (on the order of 10^{-10}) but with an order of magnitude speedup.

Properties of E We present here several interesting properties regarding the fundamental matrix, E, a central element in our approach. To our best knowledge, many of them are not shown before for the fundamental matrix of a absorbing Markov chain.

- **Nonnegativity.** For a digraph, elements of its fundamental matrix satisfies $e_{ij} \geq 0$, $1 \leq i, j \leq n$.
- **Edge reversal property.** By simply reversing all the edge directions of a digraph with a fundamental matrix E, the corresponding new fundamental matrix is equal to E^T.
- **Connectivity and Transitivity.** (i) For any edge $(i, j) \in \{1, \cdots, n\}$ in a digraph, $e_{ij} > 0$ iff there is at least one path form v_i to v_j; (ii) For any $i, j, k \in \{1, \cdots, n\}$, if $e_{ij} > 0$ and $e_{jk} > 0$, then $e_{ik} > 0$. As boundary condition we assume there is one path of length 0 from any node to itself.

Moreover, if $\max_{i,j} q_{ij} < \frac{1}{n}$, the following properties are also hold true:

- **Diagonal dominance.** For $i, j \in \{1, \cdots, n\}$ of a digraph with $i \neq j$, $e_{ii} > \max\{e_{ij}, e_{ji}\}$.
- **Triangular inequality.** For $i, j, k \in \{1, \cdots, n\}$ of a digraph with $j \neq i$ and $k \neq i$, $e_{ii} \geq \max\{e_{ij} + e_{ik} - e_{jk}, e_{ji} + e_{ki} - e_{kj}\}$.
- **Transit inequality.** For distinct indices $i, j, k \in \{1, \cdots, n\}$ of a digraph, if there exists a path from v_i to v_k and each path from v_i to v_t includes v_k, then $e_{ik} > e_{it}$.
- **Monotonicity.** Suppose the entry q_{kt} concerning the edge from v_k to v_t is increased by $\Delta q_{kt} > 0$. Then
  - (i) $\Delta e_{kt} > 0$, and for any $i, j \in \{1, \cdots, n\}$ such that $i \neq k$ or $j \neq t$ we have $\Delta e_{kt} > \Delta e_{ij}$;
  - (ii) for any $i \in \{1, \cdots, n\}$, if there is a path from v_i to v_k, then $\Delta e_{it} > \Delta e_{ik}$.

Detailed proofs are presented in Appendix A, which are adapted based on (Chebotarev and Shamis, 1998) tackling proximity measure in a more general setting.

2.1 Connections to Existing Methods

Graph Kernels, and Random Walks with Restart Algebraically our algorithm is similar to several graph kernels, including the Von Neumann Kernel $K_{VND} = \sum_{k=0}^{\infty} = (I - \alpha W)^{-1}$ (Schölkopf and Smola, 2002), and the regularized commute time kernel $K_{RCT} = (D - \alpha W)^{-1}$ (Zhou et al., 2004; Fouss et al., 2012). These kernel functions are however constructed specifically from undirected graphs (i.e. within the cone of symmetric positive definite matrices) and based on considerably different motivations and derivations. Our approach is also related to PageRank (Page et al., 1998), which resolves the issue of source nodes by teleporting random walks that introduce bi-directional edges to all node pairs with equal weights, i.e. $\bar{P} = (1 - \eta)P + \frac{\eta}{n}\mathbf{e}\mathbf{e}^T$ with $\mathbf{e}$ a $n \times 1$ vector of all ones, and η a tiny positive real. A very similar idea is also used in random walks with restart (RWR) and their variants (Tong et al., 2006): Instead of $\frac{1}{n}\mathbf{e}$ as in PageRank, they uses a vector of all

zeros except for one being 1 to indicate the node where the random walk will be restarted, or a more generic probability distribution. Note that PageRank and RWR are different from our approach. First, both operate on graphs with *irreducible* Markov chains rather than the *absorbing* Markov chains considered in our context. By definition irreducibility requires each node can be reached from any other node, i.e. a strongly connected graph – algebraically this often gives rise to a dense matrix, as shown in the teleporting operation. Second, as side-effects of introducing the teleporting operation, the input graph structure is not well preserved, and weak edge signals also tend to be washed away. In contrast our approach is able to retain the input graph structure as well as weak signals. This is more pronounced when $\tilde{Q}$ is sparse and of large size: The matrices in both methods are dense and thus demand significant amount of computation and storage efforts, while our approach is able to maintain the induced sparse matrix structure and is much more efficient in term of computation and storage.

Graph Laplacian in Undirected Graphs Our algorithm also works with *undirected* graphs as a special case (i.e. equivalent to bi-directional edges with equal weights). An interesting observation is that here our algorithm can be shown as a scaled variant of the graph Laplacian based method in (Zhou et al., 2004), which has been specifically developed for undirected graphs. This is discussed in details in Appendix A.

Partially Absorbing Random Walks (PARW) (Wu et al., 2012) It can be shown that the absorbing Markov chains considered in our context is quite general: The random walks of (Wu et al., 2012) correspond to a very special kind of such absorbing Markov chains where the submatrix of W concerning transient nodes forms a symmetric non-negative matrix. In other words, the transient nodes are inter-connected with undirected edges, while the edges from transient to absorbing nodes are still directed. Details are relegated to Appendix A.

Spanning Forest of Digraphs (Agaev and Chebotarev, 2001) The celebrated Matrix-Tree theorem has been extended to general digraphs (Chebotarev and Shamis, 1997), where the quantity $\mathcal{Q} := \left(I+\tau L\right)^{-1}$ with $L := D-W$ is shown to be the normalized counts of spanning out-forests. It turns out $\mathcal{Q}$ is a scaled version of $(I-\alpha P^T)^{-1}$, the central piece of our approach. Details are relegated to Appendix A.

2.2 Analysis

Computational complexity The complexity of Algorithm 1 is dominated by the cost of computing the affinity matrix A in (4), which can be accomplished by solving the following linear system

$$(I-\alpha P^T)A = Y.$$

For a general dense matrix P, the computational time is $O(n^3+n^2K)$. This is e.g. about the same complexity of (Zhou et al., 2005), one of our main competing methods. Fortunately, P is usually a sparse matrix in our context, which can be exploited to reduce the computational time. There are many efficient solvers for large sparse linear systems, including both direct (Davis, 2004; Demmel et al., 1999) and iterative methods (Paige and Saunders, 1982; Saad, 2003). In our implementation, we adopt the direct solver UMFPACK (Davis, 2004) which

exists as a built-in routine (for LU, backslash, and forward slash functions) in MATLAB. The specific complexity depends on the size (n), the number of non-zero entries and the sparsity pattern of P, which remains a challenging task to provide a tighter complexity measure dedicated to our context. Nevertheless, our approach is practically much more efficient comparing to state-of-the-art methods including (Zhou et al., 2005), as is empirically verified in experiments.

Error Bound Based on Transductive Rademacher Complexity A data-dependent generalization error bound is provided for the proposed algorithm, where we focus on the binary-class case for the sake of simplicity. The bound provided by our analysis is built on top of the work of (El-Yaniv and Pechyony, 2009) on transductive Rademacher complexity.

We start by reformulating our algorithm (4) as an equivalent representation

$$\mathbf{h} = E\hat{\mathbf{y}} = (I - \alpha P^T)^{-1}\hat{\mathbf{y}}, \tag{9}$$

where $\hat{\mathbf{y}}$ is the initial label vector with partial labels $\hat{\mathrm{y}}_i \in \{\pm 1\}$ for $v_i \in \mathcal{V}_l$, and $\hat{\mathrm{y}}_i = 0$ otherwise. The obtained $\mathbf{h}$ is the "soft" label vector with h_i being the "soft" label for node v_i, which will be assigned with class label $\mathrm{sign}(\mathrm{h}_i)$ when making predictions [2]. We denote by $\mathcal{H}_{out}$ the set of feasible soft label vectors generated by our algorithm (9). Since there are l labeled nodes, it follows that

$$\mathcal{H}_{out} \subseteq \mathcal{H} := \left\{ \mathbf{h} \;\middle|\; \mathbf{h} = (I - \alpha P^T)^{-1}\hat{\mathbf{y}}, \|\hat{\mathbf{y}}\|_2 \leq \sqrt{l} \right\}, \tag{10}$$

which naturally admits a *vanilla unlabeled-labelled representation* proposed in (El-Yaniv and Pechyony, 2009). We proceed with the definition of transductive Rademacher complexity.

Definition 3 *(El-Yaniv and Pechyony, 2009) Let $\mathcal{F} \subseteq \mathbb{R}^n$ and $p \in [0, 1/2]$. The transductive Rademacher complexity of $\mathcal{F}$ with parameter p is defined as*

$$R_{l,n}(\mathcal{F}, p) := \left(\frac{1}{l} + \frac{1}{n-l} \right) \mathbb{E}_{\boldsymbol{\sigma}} \left[\sup_{\mathbf{f} \in \mathcal{F}} \boldsymbol{\sigma}^T \mathbf{f} \right], \tag{11}$$

where $\boldsymbol{\sigma} = (\sigma_1, \cdots, \sigma_n)^T$ is a vector of i.i.d. random variables such that

$$\sigma_i := \begin{cases} 1, & \textit{with probability } p, \\ -1, & \textit{with probability } p, \\ 0, & \textit{with probability } 1 - 2p. \end{cases} \tag{12}$$

2. We should remark that predictions made in this way are exactly the same as the predictions made by Algorithm 1 in the binary case. Let $\mathcal{I}_1$ and $\mathcal{I}_2$ denote the index sets of labeled data from classes 1 and 2, respectively, it follows that $Y_{i1} = 1$ if $i \in \mathcal{I}_1$, $Y_{i2} = 1$ if $i \in \mathcal{I}_2$ and $Y_{ij} = 0$ otherwise; $\hat{\mathbf{y}}_i = 1$ if $i \in \mathcal{I}_1$, $\hat{\mathbf{y}}_i = -1$ if $i \in \mathcal{I}_2$ and $\hat{\mathbf{y}}_i = 0$ otherwise. Then, from equations (4) and (9) we have

$$A = \left[\sum_{i \in \mathcal{I}_1} E_{:i} \;\; \sum_{i \in \mathcal{I}_2} E_{:i} \right] \text{ and } \mathbf{h} = \sum_{i \in \mathcal{I}_1} E_{:i} - \sum_{i \in \mathcal{I}_2} E_{:i},$$

which implies that for $1 \leq i \leq n$

$$\mathrm{sign}(\mathrm{h}_i) = \arg \max_{k \in \{1,2\}} a_{ik}.$$

Different from inductive Rademacher complexity (Bartlett and Mendelson, 2002), the transductive complexity does not depend on any underlying distribution. Besides, for any label vector $\mathbf{h}$, define the *test error* as $\mathcal{L}_{l,n}(\mathbf{h}) := \frac{1}{n-l}\sum_{i=l+1}^{n}\ell(\mathrm{h}_i, \mathrm{y}_i)$ with respect to its 0/1 loss function ℓ satisfying $\ell(\mathrm{h}_i, \mathrm{y}_i) = 1$ if $\mathrm{h}_i \neq \mathrm{y}_i$ and $\ell(\mathrm{h}_i, \mathrm{y}_i) = 0$ otherwise, and define the *empirical error* of $\mathbf{h}$ as $\hat{\mathcal{L}}_{l,n}(\mathbf{h}) := \frac{1}{l}\sum_{i=1}^{l}\ell(\mathrm{h}_i, \mathrm{y}_i)$. Based on the aforementioned transductive Rademacher complexity, in what follows we present our risk bound and relegate the proof to Appendix A.

Theorem 4 *Let $\mathcal{H}_{out}$ be the set of feasible soft label vectors generated by applying* (9) *to all possible sample set $\{(v_i, \mathrm{y}_i)\}_{i=1}^{n}$. Let $c_0 := \sqrt{32\ln(4e)/3}$, $q := 1/l + 1/(n-l)$ and $s := \frac{n}{(n-1/2)(1-1/(2\max(l,n-l)))}$. For any $\delta \in (0,1)$, with probability $1-\delta$ over random draws of sample $\{(v_i, \mathrm{y}_i)\}_{i=1}^{n}$, for all $\mathbf{h} \in \mathcal{H}_{out}$,*

$$\mathcal{L}_{l,n}(\mathbf{h}) \leq \hat{\mathcal{L}}_{l,n}(\mathbf{h}) + \sqrt{\frac{2l}{n(n-l)}\|(I-\alpha P^T)^{-1}\|_F^2} + c_0 q\sqrt{\min(l, n-l)} + \sqrt{\frac{sq}{2}\ln\frac{1}{\delta}}, \quad (13)$$

It is easy to see that when $l \to \infty$, and $(n-l) \to \infty$, $s \to 1$. Then the convergence rate is determined by the slack terms $c_0 q\sqrt{\min(l, n-l)} + \sqrt{\frac{sq}{2}\ln\frac{1}{\delta}}$, which is in the order of $O\Big(\frac{1}{\sqrt{\min(l,n-l)}}\Big)$. So far we provide an transductive Rademacher bound for the binary scenario. In addition, a transductive bound based on PAC-Bayes is also provided in what follows for general multiclass setting where binary classification can be regarded as a special case. It is known that the first bound is tighter but more focused on binary classification, while the PAC-Bayes bound is more general.

PAC-Bayesian Transduction Bound In this section we present another error bound for our algorithm. This bound is a simple application of the PAC-Bayesian bound for transductive learning developed in (Derbeko et al., 2004) and can be applied to both binary-class and multi-class cases. The proof is given in Appendix A.

Theorem 5 *Let $\hat{\mathcal{L}}_{l,n}(\mathbf{h})$ and $\mathcal{L}_{l,n}(\mathbf{h})$ be the empirical error and test error, respectively, defined the same as in the previous section with respect to the 0/1 loss function ℓ. Then, for any $\delta \in (0,1)$, with probability at lest $1-\delta$ over random draws of $\mathcal{V}_l$ from $\mathcal{V}$, the following bound holds for any $\mathbf{h} \in \mathcal{H}$*

$$\mathcal{L}_{l,n}(\mathbf{h}) \leq \hat{\mathcal{L}}_{l,n}(\mathbf{h}) + \sqrt{\left(\frac{2\hat{\mathcal{L}}_{l,n}(\mathbf{h})n}{n-l}\right)\frac{ln\frac{l}{\delta} + 7ln(n+1)}{l-1} + \frac{2\left(ln\frac{l}{\delta} + 7ln(n+1)\right)}{l-1}}. \quad (14)$$

Notice that when $\hat{\mathcal{L}}_{l,n}(\mathbf{h}) = 0$ (i.e. the "realizable case") the bound converges to 0 as $l \to \infty$ and the number of unlabeled instances is a t-th ordered polynomial of l (i.e. $n - l = O(l^t)$) for any t. This is consistent with what we have previously for the data-dependant bound.

3. Experiments

Our approach is empirically evaluated in various applications, including the retinal blood vessel tracing problem and the citation problem, as well as the social network problem McAuley

and Leskovec (2012). The tracing problem involves three datasets: a synthetic dataset, as well as DRIVE (Staal et al., 2004) and STARE (Hoover et al., 2000); For the citation problem three datasets are employed: US Patent (Leskovec et al., 2005), CoRA (Macskassy and Provost, 2007) and CiteSeer (Macskassy and Provost, 2007). For social network we consider the Google+ and the Twitter datasets of McAuley and Leskovec (2012), where the goal is to identify the social circles of individual users. Our approach is compared with eight state-of-the-art methods that directly work with directed graphs:

- Network-only Bayes Classifier (NBC) (Chakrabarti et al., 1998).
- Network-only Link Based classifier (NLB) (Lu and Getoor, 2003).
- Class Distribution Relational Neighbor classifier (CDRN) (Macskassy and Provost, 2007).
- Weighted Vote Relational Neighbor classifier (WVRN) (Macskassy and Provost, 2007).
- Digraph variant of the Commute Time Kernel classifier (CTKd) (Fouss et al., 2012).
- Symmetrized Graph Laplacian (SGL) (Zhou et al., 2005).
- Zero-mode Free Laplacian (ZFL) (Wang et al., 2010).
- Sum Over Path covariance kernel (SOP) (Mantrach et al., 2010).

Out of these methods, four (NBC, NLB, CDRN, and WVRN) are implemented by NetKit (Macskassy and Provost, 2007) in Java, SOP (Mantrach et al., 2010) is obtained from the authors, while the rest (CTKd, SGL, ZFL, and Ours) are implemented by ourselves in MATLAB. Note the original Commute Time Kernel classifier (or CTKu) only works with undirected graphs. To work with digraphs, we instead replace its original undirected graph Laplacian with the symmetrized digraph Laplacian of (Chung, 2005). As a result, this variant is referred to as CTKd in this paper. To ensure fair evaluations, the internal parameters of the comparison methods are either set to as is from the authors' original source code, or as suggested by their respective authors: For example, according to (Zhou et al., 2005), the regularization parameter is set to 0.1 and the jumping factor used in teleporting random walk is set to 0.01. In particular, for the four methods implemented by NetKit, the uniform local-classifier is used as the "local" model, and for collective inference relaxation labeling has been used for NBC, CDRN, and WVRN, while iterative classification is used for NLB. This setting is reported (Macskassy and Provost, 2007) to deliver the best performance.

In term of evaluation metric, the micro-averaged accuracy (AC) (Sen and Getoor, 2007) is adopted in all experiments as the accuracy measure, which is the sum of all true positive counts divided by the total number of instances. Besides, the DIADEM score (DS) (Gillette et al., 2011) is also employed for the vessel tracing problem, which is a dedicated measure widely used by the biological tracing community. For the social network applications where there is a need to evaluate the partial correctness of predicted labels in the multi-label setting, a modified version of F_1 score Godbole and Sarawagi (2004) is used:

$$F_1 = \frac{1}{nk} \sum_{i,k} \frac{2|\tilde{y}^*_{ik} \bigcap z_{ik}|}{|\tilde{y}^*_{ik}| + |z_{ik}|} \tag{15}$$

where $\tilde{y}^*_{ik}$ and z_{ik} are predicted and true labels for the k-th label of the i-th instance.

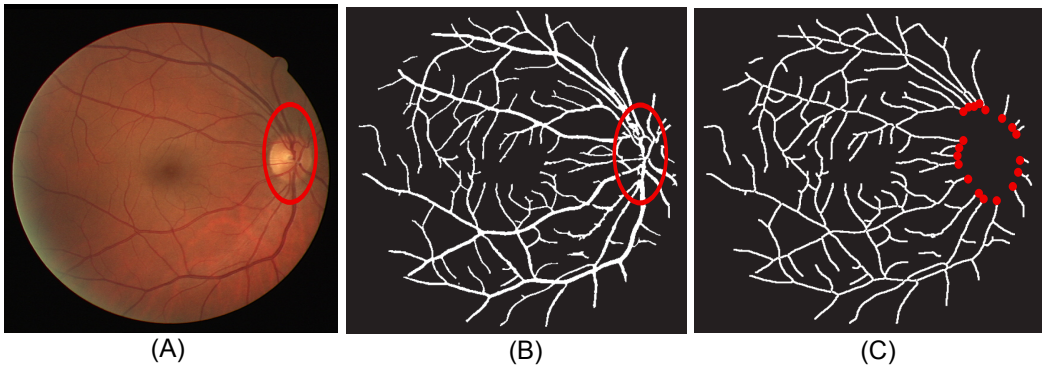

Figure 2: Preprocessing of retinal blood vessel tracing. (A) An input image from DRIVE. (B) Binary image after segmentation. (C) Image after skeleton extraction and optical disk removal. The red elliptical area in (A) and (B) is the optical disk. The red dots in (C) are tips of the *root segments* identified as those directly contacting the optical disk. Note each root segment will induce a distinct vessel tree from the graph with itself being the tree root, due to the nature of blood flow in vessels.

Retinal blood-vessel Tracing In vessel tracing, our approach is evaluated in synthetic datasets (De et al., 2014), as well as two standard testbeds, DRIVE (Staal et al., 2004) and STARE (Hoover et al., 2000). The synthetic dataset is constructed in house that contains $17,000$ synthesized retinal images with varying densities of blood vessels (which strongly correlate with the frequency of cross-over occurrences among vessel branches). Meanwhile, DRIVE dataset contains 40 retinal fundus images, and STARE has 20 fundus images. Exemplar images of the three datasets are plotted in the first row of Figure 4. Detailed protocol for creating the synthetic retinal images can be found in (De et al., 2014).

The problem of vessel tracing is to trace blood vessels by separating them into disjoint vessel trees, each starting from a unique root segment within the optical disk. The major difficulty here is to resolve the challenging cross-over issues that are abundant in the retinal datasets. This problem can be cast into a digraph-based transduction problem after the following preprocessing steps:

i) Segmentation: As illustrated in Figure 2 (A)$\rightarrow$(B), an input retinal image is segmented into a binary image, with vessel pixels being foreground and the rest as background.

ii) Skeleton map: Build a skeleton map from the binary image, and remove the optical disk area as marked within red ellipse in Figure 2(c). The tips attached to the removed optical disk are the tips of root segments, as is also presented as red dots in Figure 3(A).

iii) Skeleton to digraph: A segment is defined in the skeleton as the group of connected pixels that ends in either a junction or a tip. This segment corresponds to a node in the resulting digraph, as shown in Figure 3(A)$\rightarrow$(B). Two node is then linked with a directed edge if the two coinciding segments from the skeleton map contact and satisfy the ordering criteria of (De et al., 2014).

This produces a digraph as Figure 3(B), where red-color nodes corresponding to the root segments in skeleton map are labeled with distinct class labels, each for one particular vessel tree. The task is to propagate class labels (tree ids) to the rest unlabeled nodes. As reported in Table 1, overall our approach consistently outperforms the other methods by a

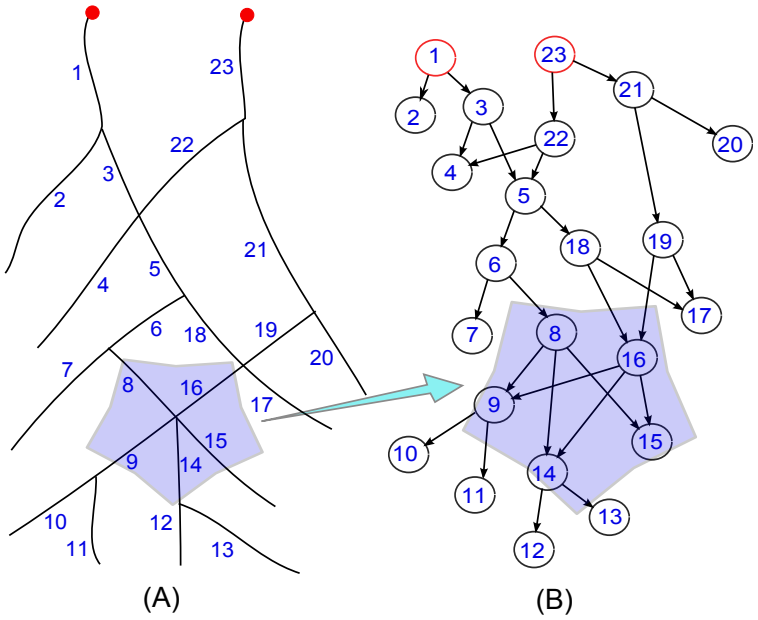

Figure 3: From skeleton to digraph. (A) A exemplar skeleton map. (B) Its digraph G. The highlighted zone of nodes are shown as an example where the corresponding directed subgraph is formed. The segments marked with red dots at their tips are the root segments, with each being regarded as the labeled node for its class. In other words, each class (corresponds to a vessel tree) has exactly its root node labeled, which corresponds to a source node in graph.

Synthetic Dataset (De et al., 2014)

	NBC	NLB	CDRN	WVRN	CTKd	SGL	SOP	ZFL	Ours
AC	0.68	0.67	0.63	0.65	0.63	0.71	0.61	0.73	**0.74**
DS	0.63	0.61	0.62	0.62	0.61	0.64	0.59	0.69	**0.71**

DRIVE (Staal et al., 2004)

	NBC	NLB	CDRN	WVRN	CTKd	SGL	SOP	ZFL	Ours
AC	0.74	0.73	0.69	0.67	0.73	0.76	0.69	0.81	**0.83**
DS	0.72	0.71	0.68	0.64	0.72	0.75	0.67	0.76	**0.77**

STARE (Hoover et al., 2000)

	NBC	NLB	CDRN	WVRN	CTKd	SGL	SOP	ZFL	Ours
AC	0.77	0.75	0.71	0.73	0.75	0.79	0.70	0.85	**0.88**
DS	0.75	0.74	0.68	0.69	0.74	0.76	0.67	0.79	**0.82**

Table 1: The micro-averaged accuracy (AC) and the average DIADEM score (DS) are reported for the synthetic dataset, as well as DRIVE and STARE.

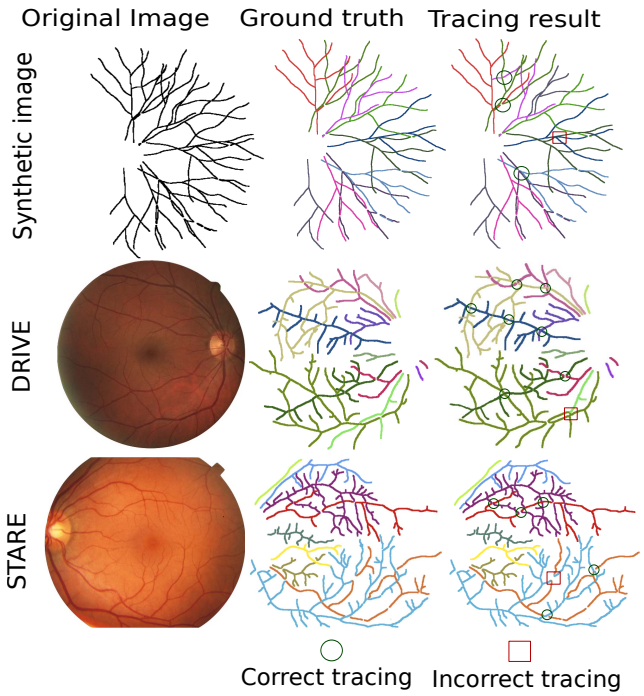

Figure 4: Exemplar retinal tracing results on Synthetic dataset, DRIVE, and STARE. The first, second and third column shows the original images, ground-truth images and tracing results respectively. Segments with the same color form a distinct vessel tree. Thus the number of colors equal to the number of classes (vessel trees). Selected correct (wrong) tracing segments are shown in green circles (red squares).

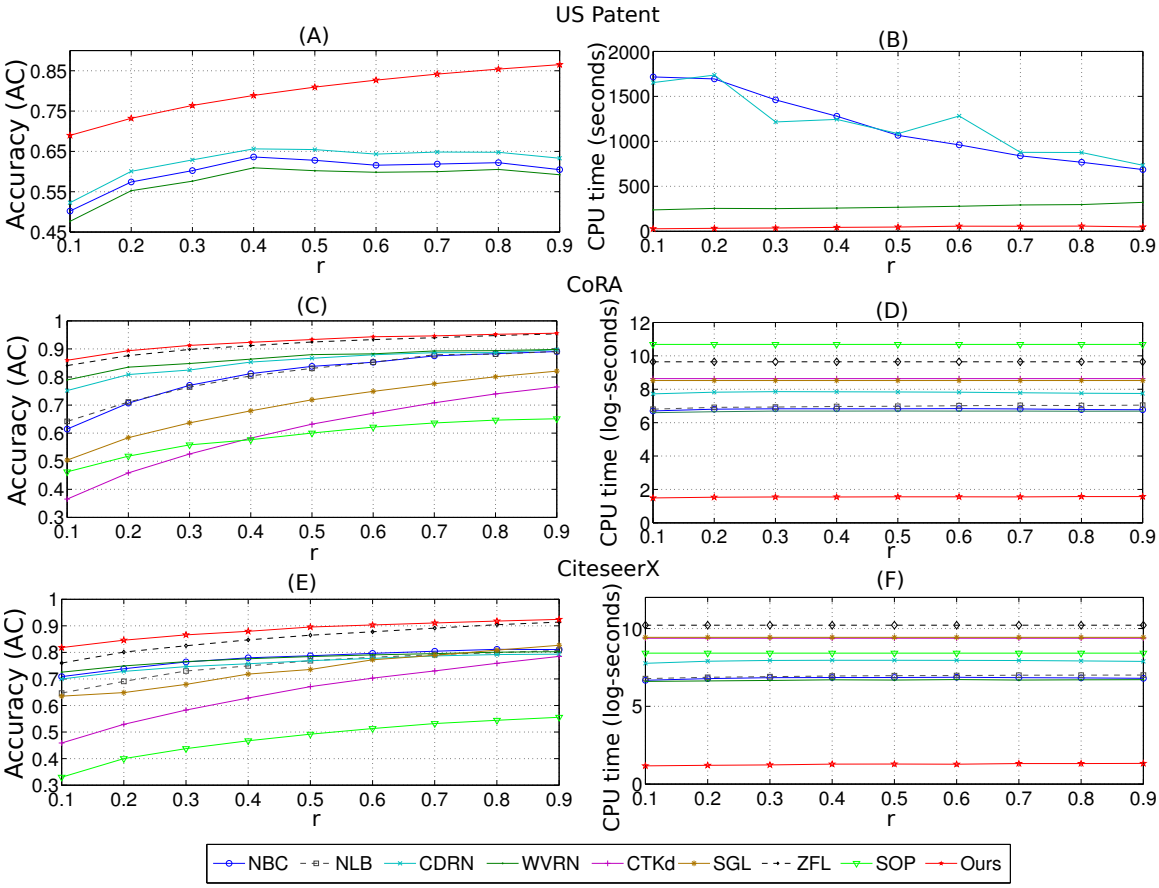

Figure 5: Comparisons of accuracy & efficiency on the citation problem (i.e. datasets of US Patent, CoRA and CiteseerX). Plots of the first column display the micro-averaged accuracy (AC) on US Patent, CoRA and CiteseerX, respectively; Plots of the second column show the corresponding CPU time spent. In all plots, the horizontal axis denotes the label ratio (percentage of labeled nodes) varying from 10% to 90% with 10% increment. See text for details.

margin. It is followed by ZFL, SGL and NBC, while WVRN and SOP tend to produce least accurate predictions. ZFL also performs reasonably well on vessel tracing problems, which is however cumbersome when deal with large matrices, as it requires to work with (and even invert) dense matrices. Exemplar images and results are also presented in Figure 4 for visual inspection. It suggests that empirically our approach delivers visually plausible tracing results when comparing to the ground-truths side-by-side, and the errors occur at those challenging spots that are often also difficult for human observers.

Citation Problem Paper citations naturally form a digraph and the aim here is to predict a prescribed topic for each of the unlabeled papers at hand, provided a few are labeled a priori. We first examine our approach on a *large-scale* dataset, US Patent (Leskovec et al., 2005), meanwhile we also conduct evaluations on the other two standard datasets: CoRA (Macskassy and Provost, 2007) and CiteseerX (Giles et al., 1998). The US Patent

dataset consists of 13 million directed edges connecting 2.7 million nodes that can be categorized into 418 distinct topics. The CoRA dataset contains a citation digraph of 2,708 nodes and 5,429 directed links (edges) on computer science research papers spanning 7 topics. CiteseerX is another citation dataset of 3,312 papers and 4,732 citations (directed edges) from 6 categories. Here the adjacency matrices are adopted as their corresponding weight matrices.

To evaluate the system performance against varying size of labeled nodes in digraphs, the following strategy is adopted: For each of the K classes, certain percentage (i.e. label ratio, also denoted as r) of instances (i.e. nodes) in this class is uniformly selected as labeled nodes – this gives one empirical data sample. This procedure is repeated 50 times to produce an averaged performance estimate. We then vary the label ratio $r$from 10% to 90% with 10% increment, and compare the averaged performance (AC) of competing methods as presented in Figure 5 first column. Note that during these experiments, when the labeled nodes are selected, the nodes with "zero-knowledge" components (Macskassy and Provost, 2007) will be temporarily removed from consideration, as are the graph nodes that have no directed path connecting to any node in $\mathcal{V}_l$. Besides, Figure 5 second column displays the average CPU time for each of the competing methods: For US Patent dataset, the timing is of a single run, while for CoRA and CiteseerX, the timing is instead recorded over 1,000 runs to ensure all timing values are above zero in the log-second scale.

Overall our approach consistently outperforms the state-of-the-arts while consuming the least amount of computational resource. For US Patent dataset, NLB, CTKd, SGL, ZFL, and SOP fail to work as these methods require dense matrices of 2.7 million by 2.7 million entries. So only our results are compared with only NBC, WVRN and CDRN on US Patent dataset. In term of accuracy, our method performs consistently the best and with a very significant gap (10%-20%) comparing to the others across different labeling ratios. The consistently superior performance of our approach still carries on for CoRA and CiteseerX datasets: ZFL becomes the second best method, which is followed by WVRN and others, while CTKd and SOP often produce the least favorable results. Note the performance of SGL, a closely related method of ours, is almost at the lower end of the middle regime of performers. We attribute this to the fact that both CoRA and WVRN are not very dense digraphs and their edge weights are quite asymmetric, which seems to be difficult for SGL, as source information is not well kept after utilizing teleporting Markov chain as well as the symmetrized graph Laplacian (Chung, 2005). Our results are also align with existing evaluations [3], although the results are not directly comparable, due to the randomized nature when sampling instances for each of the label ratios. In term of CPU time as in Figure 5 second column, our method consumes significantly less time compare to the other methods, and is with a significant gap from the second best, WVRN. On the flip side, ZFL, and SOP are the most computational intensive of all, which is closely followed by SGL. In particular, our method is shown (Figure 5 (B)) to be at least over 100 times more efficient when working with the large-scale US patent dataset, where it takes merely around 26 seconds for our approach to make predictions on this million-node dataset using a standard desktop. Note that comparing to ZFL, our method delivers consistently better results on CoRA and CiteseerX, and runs much more efficiently. In particular our method also works

3. E.g. Fig.6 of (Macskassy and Provost, 2007) on CoRA where the best performer delivers around 0.8-0.9 by varying the label ratios.

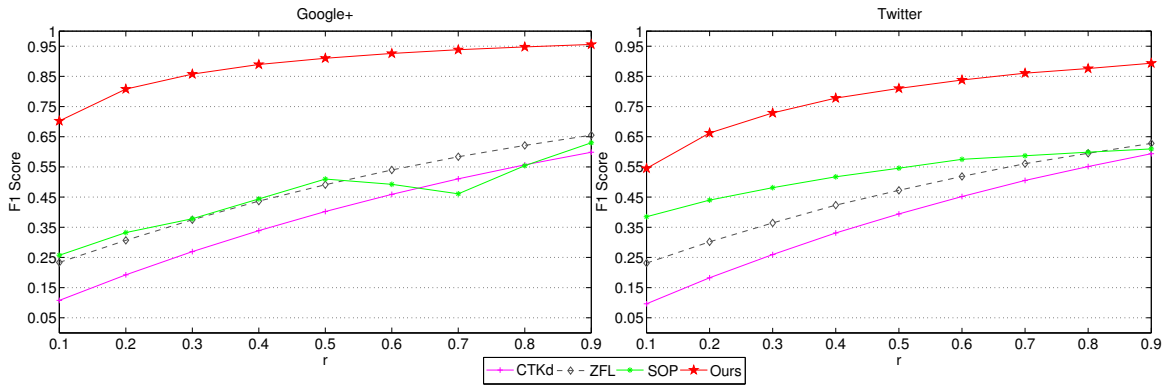

Figure 6: Comparisons of F1-Score on the multi-label problem of Google+ and Twitter datasets. In both plots, the horizontal axis denotes the label ratio (percentage of labeled nodes) varying from 10% to 90% with 10% increment. See text for details.

well with large-scale datasets such as the US Patent, which is however no possible to use ZFL.

Social Network Application It is a non-trivial task to identify social circles in social networks. Usually such a problem involves many different labels (circles) and is of large size. In particular, we consider the problem of identifying 327 social circles in the Google+ dataset, and 3,127 social circles in the Twitter dataset. both datasets are from McAuley and Leskovec (2012). The Google+ dataset consists of a graph of 1.4 million nodes and 30 million directed edges belonging to 133 users. As only part of the nodes are with their ground-truth labels, those nodes with no label information are trimmed away – we are thus left with 19,327 nodes and 3,294,465 directed edges. Similarly, the Twitter dataset has 81,306 nodes and 2.4 million directed edges from 1,000 users. After removing nodes with no label information, we obtain a digraph with 19,270 nodes and 490,667 directed edges. For experimental evaluation, the labelling ratios are varied from 10% to 90% with 10% increment, and the F_1 score in (15) are computed. NBC, NLB, CDRN and WVRN are only able to work with single-label classification problem. In the meantime, the teleporting random walks introduced in SGL tends to wash away weak signals, which seems to significantly deteriorate the performance over all label ratios. As a result, our approach are compared with three remaining methods: CTKd, ZFL and SOP, as presented in Figure 6. Our approach clearly outperforms the other three state-of-the-arts by a very large margin in both datasets. For the Google+ datset, ours produces a series of increasing F1-scores of 0.7–0.95 with the increment of label ratios r, where ZFL and SOP are the best runner-ups with combined best performance of merely 0.25–0.65 during the same range of r. CTKd seems to perform least well. These phenomenons are similarly observed for the Twitter dataset. The drop of performance in the comparison methods seems to be attributed to the combined influences of large label size and large data size (In the large-sized US patent dataset we also observe a rather significant margin between our method and the best runner-up). The superior performance of our approach, on the other hand, suggests that our approach is particularly reliable when dealing with large-sized data with many labels.

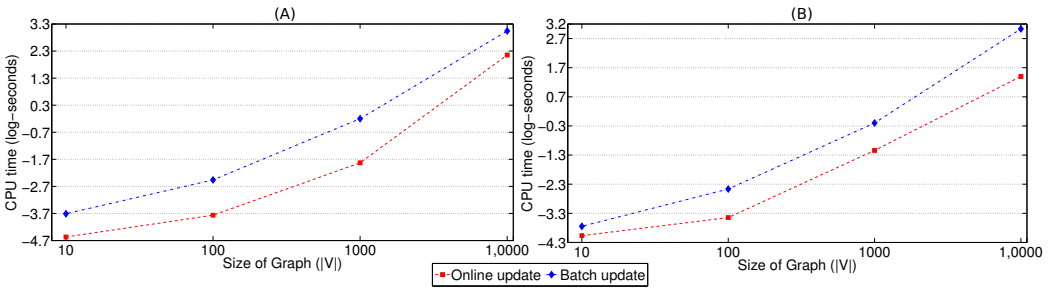

Figure 7: Empirical time-complexity of batch (3) vs. online (7,8) updates of the fundamental matrix, E. (A) and (B) show the CPU-time (log-seconds) of batch update vs. online update for changing one row using (7), and for inseting/deleting a new node with (8), respectively. See text for details.

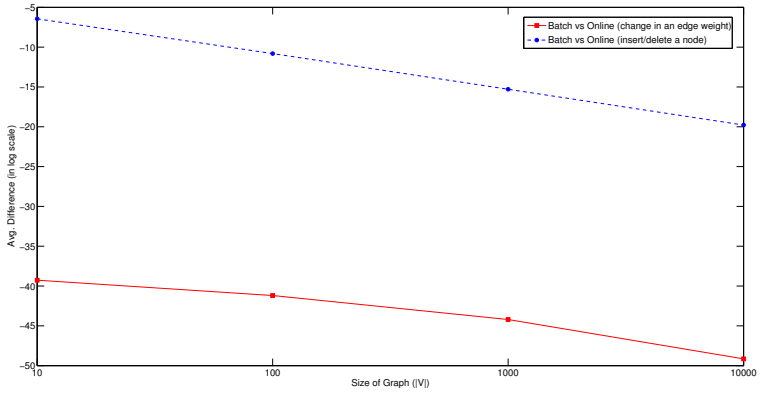

Figure 8: Averaged absolute difference between online and batch updates. The red curve (with a square mark) and the blue curve (with a star mark) shows the average differences for changing one row using (7), and for inseting/deleting a new node with (8), respectively.

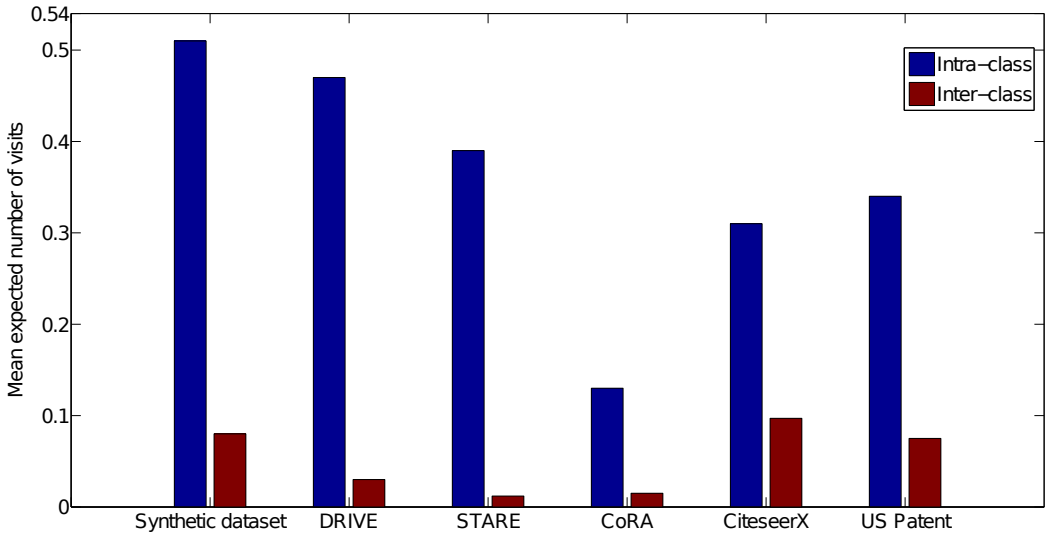

Figure 9: Empirical discriminative ability of our approach. Intra- and inter-class accumulated affinities are displayed over different datasets. Intuitively the larger the gap between intra- and inter-class, the better its performance would be. See text for details.

Empirical Time-complexity of Batch vs. Online Updates Here we focus on the dynamic graph scenario where a small fraction of the digraph structure might change over time, being either a single edge weight, or inserting/deleting a single node. In our context, this boils down to efficient computation of the fundamental matrix E. Our approach is capable of addressing these changes in E, as presented in (7) and (8) for online updates, as well as in (3) for batch update. Ideally, the online updates are expected to be carried out more efficiently and the results should be the same as of batch update. To show this, we design the following synesthetic experiments: The weight matrix of a sparse digraph of size n is randomly generated with its E matrix computed. This is followed by either changing a single edge weight, or inserting/deleting a single node from the digraph, which subsequently gives E'. Its respectively online update is then computed by (7) or (8), vs. the batch update of (3). The above process is repeated 20 times, for each of the following four different digraph sizes, namely $n \in \{10, 100, 1000, 10, 000\}$, and the median running time is displayed in Figure 7(A) and (B). Note that this comparison is not entirely fair, where our implementation is less favored: To compute (3) for batch update, the Matlab implementation of UMFPACK direct solver is highly optimized and runs on multi-cores, while our implementation of the online updates, namely (7) and (8) are in Matlab script as is (without any optimization). Nevertheless, as presented in Figure 7 the online updates runs always an order of magnitude faster. Besides, empirically the numerical difference value between batch and online updates are numerically negligible. As displayed in Figure 8, on average the absolute difference value is always below $10^{-}5$ in the above mentioned experiments. In addition, this numerical error decreases dramatically with the increase of digraph sizes.

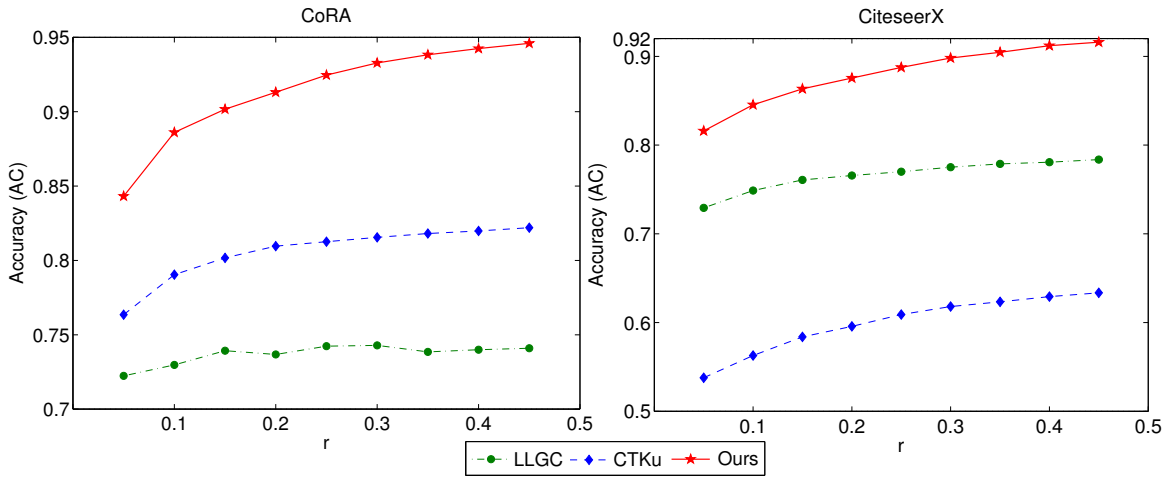

Figure 10: Comparison with state-of-the-art methods based on undirected graphs.

Analyzing Discriminative Ability of Our Approach Further, we compare the intra- and inter-class accumulated affinity scores over different datasets, which offers an empirical explanation for the discriminative ability of our approach. The results displayed in Figure 9 are obtained as follows: For each non-zero (i, j)-th entry in E there is a directed path connected both nodes. Now group all entries in E into two sets: Those with both nodes belonging to the same class (i.e. intra-class), and the rest that each from a different classes (i.e. inter-class). Then accumulate the scores within each set and normalize – which produces the final scores. The intra-class score is expected to outnumber the inter-class one, and the larger the gap (or ratio) between the two suggests a better discriminative ability on the particular dataset. As revealed in Figure 9, the ratios are all very large across various datasets used in this paper, which indeed suggests that our algorithm is expected to deliver good performance regardless of any particular set of input labels.

Comparison with Undirected-graph based Methods So far we have compared our approach to a number of methods that can directly work with digraphs. One may still wonder how conventional undirected-graph based methods would perform in our context. For this purpose we implement in matlab two state-of-the-art such methods, namely the original Commute Time Kernel classifier (CTKu) (Fouss et al., 2012), and the Learning with Local and Global Consistency (LLGC) method in Zhou et al. (2004), both operate on undirected graphs. The comparison is performed on CoRA and CiteseerX datasets with results presented in Figure 10 when the label ratios are changed from 0.1 to 0.9. Our approach maintains a clear performance gap of about 10% overall for both datasets. LLGC and CTKu alternate in both datasets as being the runner-up, with a further margin of around 10% over the worst performing one of the three methods.

The Effect of α We also provide empirical analysis to study the effect of varying α value to the performance of the proposed system: As presented in Figures 11, our performance is rather stable against changing α values varying from .01 to .99 on various datasets. This observation is further confirmed in Figure 12 with varying label ratios, where different α

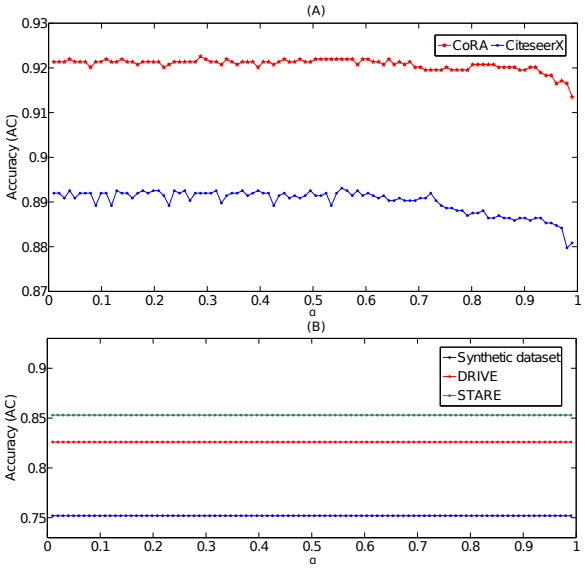

Figure 11: Robustness of our system vs. changing α values between .01 and .99. (A) For CoRA and CiteseerX, the performance or our system is rather stable (with around .001 variation) when α is within .01 and 0.9, and start to decrease slightly (around .01 variation) when α value goes beyond .9. (B) The performance remains constant regardless of α values in vessel tracing problems.

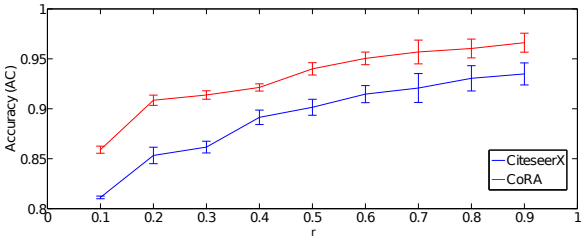

Figure 12: Robustness of our system with respect to varying label ratio. The error bar of each labeling ratio (r) displays 5 – 95 percentile of accuracy when α values are systematically sampled between .01 and .99 with an .01 increment. The narrow deviations from median as shown in the error bar (usually less than 2%) clearly suggest that our system is rather stable against changes of α values.

values usually result in less than 2% variations in its performance. The insensitive pattern of α is experienced throughout empirical experiments. This motivate us to simply fix α to certain value (0.1) during the rest experiments. We note in the passing that some performance degradation is to be expected as α taking extreme values being too close to either 0 or 1, since which renders E to be too close to either the identity matrix or an ill-conditioned matrix, respectively.

4. Conclusion and Outlook

A novel random walk approach is proposed on digraphs that is able to preserve edge directions and is shown to perform competitively against the state-of-the-art methods. For future work, we plan to explore broader scope of applications, as well as to generalize to work with problems with structured labels.

Acknowledgments

We would like to acknowledge support for this project from A*STAR JCO and IAF grants.

Appendix A. Proof of Proposition 1

Proof We know (Kemeny and Snell, 1976) that the fundamental matrix of $\tilde{Q}$ is $E = \sum_{t=0}^{\infty} Q^t$, and are left to show that $(I-\alpha P^T)^{-1}$ exists, and $E = (I-\alpha P^T)^{-1}$. $(I-\alpha P^T)^{-1}$ exists, since its spectral radius $\rho(P)$ defined as the absolute value of its largest eigenvalue is always 1, and $\alpha < \rho(P)^{-1}$ since $\alpha \in (0,1)$. we also have $Q^\infty = (\alpha P^T)^\infty = 0$ and the series $I + Q + Q^2 + \ldots$ will converge to $(I-\alpha P^T)^{-1}$. ■

Proof of Proposition 2

Proof (i) We focus only on the change in q_{ij}. The difference between Q and Q' is given by

$$Q' - Q = \Delta q_{ij} \varepsilon_i \varepsilon_j^T,$$

where ε_i (ε_j) is a column vector with the i-th (j-th) entry being 1 and all other entries being 0. By the Sherman-Morrison-Woodbury formula (Golub and Loan, 1996), we have

$$\begin{aligned} E' =& (I-Q')^{-1} = (I - Q - \Delta q_{ij}\varepsilon_i\varepsilon_j^T)^{-1} \\ =& (I-Q)^{-1} + \frac{\Delta q_{ij}}{1 - \Delta q_{ij}\varepsilon_j^T (I-Q)^{-1}\varepsilon_i} (I-Q)^{-1}\varepsilon_i\varepsilon_j^T (I-Q)^{-1} \\ =& E + \frac{\Delta q_{ij}}{1 - \Delta q_{ij} e_{ji}} E_{:i} E_{j:}, \end{aligned}$$

which completes the proof of part (i).

(ii) The update of E is obtained by noting that

$$Q' - Q = \varepsilon_i \Delta Q_{i:}$$

and applying the Sherman-Morrison-Woodbury formula as in part (i).

(iii) By the definition of E, we have

$$\begin{aligned} E' =& (I-Q')^{-1} = \begin{bmatrix} I-Q & -u \\ -v^T & 1-q \end{bmatrix}^{-1} \\ =& \begin{bmatrix} (I-Q)^{-1} + \gamma (I-Q)^{-1} u v^T (I-Q)^{-1} & \gamma (I-Q)^{-1} u \\ \gamma v^T (I-Q)^{-1} & \gamma \end{bmatrix} \\ =& \begin{bmatrix} E + \gamma (Eu)(v^T E) & \gamma (Eu) \\ \gamma (v^T E) & \gamma \end{bmatrix}, \end{aligned}$$

where $\gamma = \frac{1}{(1-q) - v^T (I-Q)^{-1} u} = \frac{1}{(1-q) - v^T E u}$.

■

Proofs for Properties of E

The first two properties, namely nonnegativity and edge reversal property follow directly from the definition of E. We thus omit their proofs and focus on the proofs of the remaining properties.

Proof of Connectivity and Transitivity

Proof It is trivial when $i = j$, so we concentrate on the case that $i \neq j$.

" $\Rightarrow$" If $e_{ij} > 0$, from Proposition 1, there exist some $t \geq 1$ such that $(Q^t)_{ij} > 0$, and

$$(Q^t)_{ij} = \sum_{i_1, i_2, \cdots, i_{t-1}} q_{ii_1} q_{i_1 i_2} \cdots q_{i_{t-1} j} > 0.$$

Since each term in the summation is nonnegative, there exits at least one term $q_{ii_1} q_{i_1 i_2} \cdots q_{i_{t-1} j} > 0$, which implies that $v_i \to v_{i_1} \to \cdots \to v_{i_{t-1}} \to v_j$ is a path from v_i to v_j.

" $\Rightarrow$" If there exists a path from v_i to v_j, without loss of generality, we represent this path as $v_i \to v_{i_1} \to \cdots \to v_{i_{t-1}} \to v_j$, then $q_{ii_1} q_{i_1 i_2} \cdots q_{i_{t-1} j} > 0$, which implies that $(Q^t)_{ij} > 0$. Hence, $e_{ij} > 0$.

■

Proof of Diagonal Dominance

Proof By reversal property, we only need to prove $e_{ii} > e_{ij}$. Without loss of generality, we assume $i = 1$. Consider the digraph $G^{(1)}$ constructed by removing all edges directed to v_1 from the completed digraph [4] with the weight of each edge being $q_{max} := \max_{i,j} q_{ij}$, we have

$$q_{ij}^{(1)} = \begin{cases} q_{max}, \text{ if } i \neq j \text{ and } j > 1, \\ 0, \text{ otherwise }, \end{cases}$$

which leads to

$$e_{11}^{(1)} = 1, \ e_{1j}^{(1)} = \frac{q_{max}}{1 - q_{max}(n-2)} \text{ if } j > 1, \ e_{i1}^{(1)} = 0 \text{ if } i > 1.$$

Since $q_{max} < \frac{1}{n}$, it follows that $e_{11}^{(1)} > e_{1j}^{(1)}$. For $t > 1$, reduce the weight $q_{kt}^{(1)}$ by the amount of $\Delta q_{kt}^{(1)}$ such that $q_{kt}^{(1)} - \Delta q_{kt}^{(1)} = q_{kt}$, resulting a new graph $G^{(2)}$. From Proposition 2, we get

$$E^{(2)} - E^{(1)} = -\frac{\Delta q_{kt}^{(1)}}{1 + \Delta q_{kt}^{(1)} e_{tk}^{(1)}} E_{:k}^{(1)} E_{t:}^{(1)},$$

which implies that $e_{11}^{(2)} = 1$, $e_{1j}^{(2)} \leq e_{1j}^{(1)} < e_{11}^{(1)} = e_{11}^{(2)}$ if $j > 1$ and $e_{i1}^{(2)} = 0$ if $i > 1$. Repeat this process, we can eventually get a new graph $G^{(3)}$ such that $e_{11}^{(3)} = 1$, $e_{1j}^{(3)} < e_{11}^{(3)}$ if $j > 1$, $e_{i1}^{(3)} = 0$ if $i > 1$, and the only difference between $G^{(3)}$ and G is the lack of edges directed to v_1 in $G^{(3)}$. Now, add an edge with weight q_{s1} $(s > 1)$ from v_s to v_1 to $G^{(3)}$ and denote the resulting graph as $G^{(4)}$, then

$$E^{(4)} - E^{(3)} = -\frac{q_{s1}}{1 - q_{s1} e_{1s}^{(3)}} e_{:s}^{(3)} e_{1:}^{(3)},$$

4. By complete graph, we refer to the graph with edges in two directions between any two nodes.

which implies that

$$e_{11}^{(4)} = \frac{e_{11}^{(3)}}{1 - q_{s1}e_{1s}^{(3)}}, \quad e_{1j}^{(4)} = \frac{E_{1j}^{(3)}}{1 - q_{s1}E_{1s}^{(3)}}.$$

Thus,

$$e_{11}^{(4)} - e_{1j}^{(4)} = \frac{e_{11}^{(3)} - e_{1j}^{(3)}}{1 - q_{s1}e_{1s}^{(3)}} > 0, \text{ if } j > 1.$$

Repeat this process, we can eventually get the original graph G and $e_{11} > e_{1j}$ if $j > 1$, which completes the proof. ■

Proof of the Triangular Inequality

Proof Similar to the proof of diagonal dominance, we only need to prove $e_{ii} \geq e_{ij}+e_{ik}-e_{jk}$, and, without loss of generality, assume $i = 1$. Let $G^{(1)}$ be the digraph constructed by removing all edges directed to v_1 from the completed digraph with the weight of each edge being $\frac{1}{n}$. Then,

$$e_{11}^{(1)} = 1, \ e_{1j}^{(1)} = \frac{1}{2} \text{ if } j > 1, \ e_{i1}^{(1)} = 0 \text{ if } i > 1,$$

which lead to $e_{11}^{(1)} - (e_{1j}^{(1)} + e_{1k}^{(1)}) = 0$, and

$$e_{11}^{(1)} - (e_{1j}^{(1)} + e_{1k}^{(1)} - e_{jk}^{(1)}) = e_{jk}^{(1)} \geq 0.$$

For $t > 1$, reduce the weight $q_{kt}^{(1)}$ by the amount of $\Delta q_{kt}^{(1)}$ such that $\frac{1}{n} - \Delta q_{kt}^{(1)} = q_{kt}$, resulting a new graph $G^{(2)}$. From Proposition 2, we get

$$\begin{aligned}
e_{11}^{(2)} =& e_{11}^{(1)}, \\
e_{1j}^{(2)} =& e_{1j}^{(1)} - \frac{\Delta q_{kt}^{(1)} e_{1k}^{(1)}}{1 + \Delta q_{kt}^{(1)} e_{tk}^{(1)}} e_{tj}^{(1)} \leq e_{1j}^{(1)} \text{ if } j > 1, \\
e_{i1}^{(2)} =& 0 \text{ if } i > 1,
\end{aligned}$$

which imply $e_{11}^{(2)} - (e_{1j}^{(2)} + e_{1k}^{(2)}) \geq e_{11}^{(1)} - (e_{1j}^{(1)} + e_{1k}^{(1)}) = 0$, and

$$e_{11}^{(2)} - (e_{1j}^{(2)} + e_{1k}^{(2)} - e_{jk}^{(2)}) \geq e_{jk}^{(2)} \geq 0.$$

Repeat this process, we can eventually get a new graph $G^{(3)}$ such that $e_{11}^{(3)} = 1$, $e_{i1}^{(3)} = 0$ if $i > 1$, $e_{11}^{(3)} - (e_{1j}^{(3)} + e_{1k}^{(3)}) \geq 0$, and the only difference between $G^{(3)}$ and G is the lack of edges directed to v_1 in $G^{(3)}$. Now, add an edge with weight q_{s1} $(s > 1)$ from v_s to v_1 to $G^{(3)}$ and denote the resulting graph as $G^{(4)}$, then

$$e_{11}^{(4)} = \frac{e_{11}^{(3)}}{1 - q_{s1}e_{1s}^{(3)}}, \ e_{1j}^{(4)} = \frac{e_{1j}^{(3)}}{1 - q_{s1}e_{1s}^{(3)}} \text{ if } j > 1.$$

Thus,

$$e_{11}^{(4)} - (e_{1j}^{(4)} + e_{1k}^{(4)}) = \frac{e_{11}^{(3)} - (e_{1j}^{(3)} + e_{1k}^{(3)})}{1 - q_{s1}e_{1s}^{(3)}} \geq 0.$$

Repeat this process, we can eventually get the original graph G and

$$\begin{aligned} e_{11} - (e_{1j} + e_{1k} - e_{jk}) =& e_{jk} + \Big((e_{11} - (e_{1j} + e_{1k})\Big) \\ \geq& e_{jk} \geq 0, \end{aligned}$$

which completes the proof. ■

Remark 6 *The diagonal dominance and triangular inequality can be applied to construct a metric on node set $\mathcal{V}$. Indeed, define a function $\mathcal{M} : \mathcal{V} \times \mathcal{V} \to \mathbb{R}$ as*

$$\mathcal{M}(v_i, v_j) := e_{ii} + e_{jj} - e_{ij} - e_{ji},$$

then we can prove that $\mathcal{M}$ is a metric on $\mathcal{V}$ (i.e., it satisfies the axioms of a metric).

Proof of Transit Inequality

Proof We prove this result by contradiction. Suppose there exist digraphs that violate the transit inequality. Let $G^{(1)}$ be the digraph with the minimum number of edges among the digraphs that violate the transit inequality. It follows that $G^{(1)}$ has a path from v_i to v_k and every path from v_i to v_t ($t \neq k$) includes v_k, but $e_{ik}^{(1)} \leq e_{it}^{(1)}$.

We first show that there exist at least one path from v_i to v_k that has more than one edges. Otherwise, every path from v_i to v_k has only one edge. Considering the ik-entry of the matrices on both sides of the equality $(I - Q^{(1)})E^{(1)} = I$, we have

$$e_{ik}^{(1)} = (Q^{(1)}E^{(1)})_{ik} = \sum_{j=1}^{n} q_{ij}^{(1)} e_{jk}^{(1)} = q_{ik}^{(1)} e_{kk}^{(1)},$$

since $q_{ij}^{(1)} e_{jk}^{(1)} = 0$ if $j \neq k$. (Otherwise, there is one path from v_i to v_k having more than one edge.) Similarly, we have $e_{it}^{(1)} = q_{ik}^{(1)} e_{kt}^{(1)}$. Thus, by diagonal dominance,

$$e_{ik}^{(1)} - e_{it}^{(1)} = q_{ik}^{(1)}(e_{kk}^{(1)} - e_{kt}^{(1)}) > 0,$$

which is a contradiction to the construction of $G^{(1)}$.

Let (v_i, v_j) be the first edge of some path from v_i to v_k such that $j \neq k$, and $G^{(2)}$ be the digraph obtained by removing the (v_i, v_j) edge from $G^{(1)}$. Then,

$$\begin{aligned} \Delta e_{ik} =& e_{ik}^{(2)} - e_{ik}^{(1)} = -\frac{q_{ij}^{(1)} e_{ii}^{(1)}}{1 + q_{ij}^{(1)} e_{ji}^{(1)}} e_{jk}^{(1)}, \\ \Delta e_{it} =& e_{it}^{(2)} - e_{it}^{(1)} = -\frac{q_{ij}^{(1)} e_{ii}^{(1)}}{1 + q_{ij}^{(1)} e_{ji}^{(1)}} e_{jt}^{(1)}. \end{aligned}$$

If there is no path from v_i to v_k, then $e_{ik}^{(2)} = 0$, $e_{it}^{(2)} = 0$, and

$$\Delta e_{ik} - \Delta e_{it} = e_{it}^{(1)} - e_{ik}^{(1)} \geq 0.$$

If there is some path from v_i to v_k, then $e_{ik}^{(2)} > e_{it}^{(2)}$ (Otherwise, $G^{(2)}$ also violates the transit inequality but has less edges than $G^{(1)}$, which is a contradiction.), which leads to

$$\Delta e_{ik} - \Delta e_{it} = (e_{ik}^{(2)} - e_{it}^{(2)}) + (e_{it}^{(1)} - e_{ik}^{(1)}) > 0.$$

In both cases, we have $\Delta e_{ik} - \Delta e_{it} \geq 0$, which together with

$$\Delta e_{ik} - \Delta e_{it} = \frac{q_{ij}^{(1)} e_{ii}^{(1)}}{1 + q_{ij}^{(1)} e_{ji}^{(1)}} (e_{jt}^{(1)} - e_{jk}^{(1)}),$$

implies $e_{jt}^{(1)} \geq e_{jk}^{(1)}$. Thus,

$$e_{jt}^{(2)} = \frac{e_{jt}^{(1)}}{1 + q_{ij}^{(1)} e_{ji}^{(1)}} \geq \frac{e_{jk}^{(1)}}{1 + q_{ij}^{(1)} e_{ji}^{(1)}} = e_{jk}^{(2)}.$$

Since $G^{(2)}$ has a path from v_j to v_k, every path from v_j to v_t includes v_k and $e_{jk}^{(2)} \leq e_{jt}^{(2)}$, it follows that $G^{(2)}$ also violates the transit inequality but has less edges than $G^{(1)}$, which is a contradiction to the construction of $G^{(1)}$. ■

Proof of Monotonicity

Proof (i) From Proposition 2, we have

$$\Delta e_{kt} = \frac{\Delta q_{kt}}{1 - \Delta q_{kt} e_{tk}} e_{kk} e_{tt}, \quad \Delta e_{ij} = \frac{\Delta q_{kt}}{1 - \Delta q_{kt} e_{tk}} e_{ik} e_{tj}.$$

Thus, $\Delta e_{kt} > 0$ and

$$\begin{aligned} \Delta e_{kt} - \Delta e_{ij} =& \frac{\Delta q_{kt}}{1 - \Delta q_{kt} e_{tk}} (e_{kk} e_{tt} - e_{ik} e_{tj}) \\ =& \frac{\Delta q_{kt}}{1 - \Delta q_{kt} e_{tk}} \Big((e_{kk} - e_{ik}) e_{tt} + e_{ik} (e_{tt} - e_{tj}) \Big) \\ >& 0, \end{aligned}$$

if $i \neq k$ or $j \neq t$, due to the diagonal dominance.

(ii) Similar to case (i), we have

$$\Delta e_{it} = \frac{\Delta q_{kt} e_{ik}}{1 - \Delta q_{kt} e_{tk}} e_{tt}, \quad \Delta e_{ik} = \frac{\Delta q_{kt} e_{kk}}{1 - \Delta q_{kt} e_{tk}} e_{tk},$$

which imply

$$\Delta e_{it} - \Delta e_{ik} = \frac{\Delta q_{kt} e_{ik}}{1 - \Delta q_{kt} e_{tk}} (e_{tt} - e_{tk}) > 0.$$

■

Connections to Graph Laplacian in undirected Graphs

Here we shown that when operating as random walks on undirected graphs, our algorithm is equivalent to a scaled variant of the graph Laplacian method of (Zhou et al., 2004). For an undirected graph G, denote $S = D^{-\frac{1}{2}} W D^{-\frac{1}{2}}$, and define $P = WD^{-1}$, where $W = [w_{ij}]$ is a symmetric matrix and $D = \mathrm{diag}(d_1, \cdots, d_n)$, with $d_i = \sum_j w_{ij}$. Now consider applying our algorithm (i.e. (4) and (5)) on undirected graph G. Since

$$A = (I - \alpha P^T)^{-1} Y = D^{-\frac{1}{2}} (I - \alpha S)^{-1} D^{\frac{1}{2}} Y,$$

we have

$$D^{\frac{1}{2}} A = (I - \alpha S)^{-1} \Big(D^{\frac{1}{2}} Y \Big).$$

Notice that since the goal is to choose the best element from the current row i as in (5), the result will not change by multiplying an additional constant $d_i^{\frac{1}{2}}$ to all elements in the row. Define $\hat{\mathrm{A}} := D^{\frac{1}{2}} \mathrm{A}$, and let $\hat{Y} := D^{\frac{1}{2}} Y$ we now have

$$\hat{A} = (I - \alpha S)^{-1} \hat{Y},$$

which recovers the update formula of (Zhou et al., 2004), with the only difference that instead of Y, $\hat{Y}$ is used here as a row-wise scaled variant.

Connections to Partially Absorbing Random Walks (PARW) (Wu et al., 2012)

The random walks considered in (Wu et al., 2012) deal with a *special* form of *absorbing Markov chains* where the submatrix of its weight matrix concerning transient nodes forms a symmetric non-negative matrix with diagonal entries taking zero values. More formally, denote this submatrix as

$$W_P = \begin{pmatrix} 0 & w_{1\,2} & \cdots & w_{1\,n} \\ w_{2\,1} & 0 & \cdots & w_{2\,n} \\ \cdots & \cdots & \cdots & \cdots \\ w_{n\,1} & \cdots & w_{n\,n-1} & 0 \end{pmatrix},$$

which is a $n \times n$ symmetric non-negative matrix with zero diagonal values. Let $\Lambda_P = \mathrm{diag}(\lambda_1, \cdots, \lambda_n)$ with $\lambda_i > 0 \ \forall i$, and define $\lambda_{\mathbf{P}} = \mathrm{vec}(\Lambda_P)$, where the operator $\mathrm{vec}(\cdot)$ extracts the diagonal elements of the input matrix to produce a column vector. The weight matrix of the PARW family proposed in (Wu et al., 2012) can be regarded as an extended matrix of W_P by introducing an additional absorbing node, as

$$\tilde{W}_P \ = \ \left(\begin{array}{c|c} W_P & \lambda_{\mathbf{P}} \\ \hline 0 & 1 \end{array} \right),$$

with 0 here referring to a $1 \times n$ vector of zero values. Define the degree matrix $D_P = \mathrm{diag}(d_1, \cdots, d_n)$ with each element computed as the sum of the corresponding row of W_P, $d_i = \sum_j w_{i\,j}$. denote the (sub-) graph Laplacian $L_P = D_P - W_P$, and let $P_W = (\Lambda_P +$

$D_P)^{-1}W_P$, and $P_\lambda = (\Lambda_P + D_P)^{-1}\Lambda_P$. At this point, we are ready to obtain the *probability transition matrix*:

$$\tilde{P}_P \quad = \quad \left(\begin{array}{c|c} P_W & \mathrm{vec}(P_\lambda) \\ \hline 0 & 1 \end{array}\right),$$

which is exactly the same form as of $\tilde{Q}$ defined earlier in Equation (1) of our approach. Note that the random walks considered in (Wu et al., 2012) is a *special* form of (1) with W_P confined to being a symmetric matrix with zero diagonal entries. Following Proposition 1, its fundamental matrix becomes

$$E_P = \sum_{t=0}^{\infty} \big(P_W\big)^t = \big(I - (\Lambda_P + D_P)^{-1}W_P\big)^{-1} = \big(\Lambda_P + L_P\big)^{-1}\big(\Lambda_P + D_P\big).$$

It is interesting to observe that the absorption probability matrix, A_P, proposed and discussed in (Wu et al., 2012) can be related to E_P as

$$A_P = \sum_{t=0}^{\infty} \big(P_W\big)^t P_\Lambda = E_P\Big[\big(\Lambda_P + D_P\big)^{-1}\Lambda_P\Big].$$

Interestingly, it corresponds to a special form of the absorbing probabilities of the Markov chain (see e.g. Theorem 3.3.7 of Kemeny and Snell, 1976).

Connections to Spanning Forest of Digraphs

Following (Chebotarev and Shamis, 1997), let $L := D - W$, and denote the forest matrix $\mathcal{Q} := \big(I + \tau L\big)^{-1}$. Suppose $\mathcal{F}$ is the set of all spanning forests of digraph G and $\mathcal{F}^{ij}$ the set of spanning forests containing edge $i \leftarrow j$. It has been shown in (Chebotarev and Shamis, 1997; Agaev and Chebotarev, 2001) that each (i,j)-th entry of $\mathcal{Q} = [q_{ij}]$ concerns the normalized counts of spanning out-forests, as $q_{ij} = \frac{\epsilon(\mathcal{F}^{ji})}{\epsilon(\mathcal{F})}$, with $\epsilon(\cdot)$ denoting the count of specified forests.

Further, denote $P^T = I - \mu L$, $\mu > 0$, and let $q = \big(1 + \frac{\tau}{\mu}\big)^{-1}$, it can be easily shown that

$$\mathcal{Q} = q\big(I - \frac{\tau}{\mu + \tau}P^T\big)^{-1}.$$

In other words, $\mathcal{Q}$ is a scaled version of $(I - \alpha P^T)^{-1}$, with $\alpha := \frac{\tau}{\mu+\tau}$.

Proof of Theorem 4

We start by stating the risk bound developed in (El-Yaniv and Pechyony, 2009).

Theorem 7 *(El-Yaniv and Pechyony, 2009) For a transductive learning algorithm, let $\mathcal{F}$ be the set of all soft labels of the algorithm obtained by applying it to all possible sample $\{(v_i, \mathrm{y}_i)\}_{i=1}^n$. Let c_0, q and s be defined the same way as in Theorem 4. For any $\delta \in (0,1)$, with probability $1-\delta$ over random draws of sample $\{(v_i, \mathrm{y}_i)\}_{i=1}^n$, for all $\mathbf{f} \in \mathcal{F}$,*

$$\mathcal{L}_{l,n}(\mathbf{f}) \le \hat{\mathcal{L}}_{l,n}(\mathbf{f}) + R_{l,n}(\mathcal{F}, p_0) + c_0 q\sqrt{\min(l, n-l)} + \sqrt{\frac{sq}{2}\ln\frac{1}{\delta}}, \tag{F.1}$$

where $p_0 = \frac{l(n-l)}{n^2} < \frac{1}{2}$.

This risk bound is quite general and can be applied to estimate the generalization error for a suite of transductive learning algorithms if one can find the transductive Rademacher complexity $R_{l,n}(\mathcal{F}, p_0)$ of the hypothesis set $\mathcal{F}$. Fortunately, in what follows we show that for the hypothesis set $\mathcal{H}_{out}$, the transductive Rademacher complexity $R_{l,n}(\mathcal{H}_{out}, p_0)$ can be found efficiently, which consequentially leads to the generalization error bound for our algorithm. From Definition 3, we notice that

$$R_{l,n}(\mathcal{H}_{out}, p_0) \leq R_{l,n}(\mathcal{H}, p_0), \text{ if } \mathcal{H}_{out} \subseteq \mathcal{H}. \tag{F.2}$$

In other words, by comparing Theorem 7 and Theorem 4, it is sufficient to prove

$$R_{l,n}(\mathcal{H}, p_0) \leq \sqrt{\frac{2l}{n(n-l)}\|(I - \alpha P^T)^{-1}\|_F^2}. \tag{F.3}$$

Note $E = (I - \alpha P^T)^{-1}$, and for convenience denote $E_{i,:}$ as the ith row of E. From the Definition 3, we have that

$$\begin{aligned}
R_{l,n}(\mathcal{H}, p_0) =& q\mathbb{E}_{\boldsymbol{\sigma}}\left[\sup_{\mathbf{h}\in\mathcal{H}} \boldsymbol{\sigma}^T\mathbf{h}\right] \\
=& q\mathbb{E}_{\boldsymbol{\sigma}}\left[\sup_{\|\hat{\mathbf{y}}\|\leq\sqrt{l}} \sum_{i=1}^n \sigma_i \langle E_{i,:}, \hat{\mathbf{y}}\rangle\right] \\
=& q\mathbb{E}_{\boldsymbol{\sigma}}\left[\sup_{\|\hat{\mathbf{y}}\|\leq\sqrt{l}} \left\langle \sum_{i=1}^n \sigma_i E_{i,:}, \hat{\mathbf{y}}\right\rangle\right] \\
=& q\sqrt{l}\mathbb{E}_{\boldsymbol{\sigma}}\left[\left\|\sum_{i=1}^n \sigma_i E_{i,:}\right\|_2\right] \\
=& q\sqrt{l}\mathbb{E}_{\boldsymbol{\sigma}}\left[\sqrt{\sum_{i,j=1}^n \sigma_i\sigma_j \langle E_{i,:}, E_{j,:}\rangle}\right] \\
\leq& q\sqrt{l}\sqrt{\sum_{i,j=1}^n \mathbb{E}_{\boldsymbol{\sigma}}[\sigma_i\sigma_j] \langle E_{i,:}, E_{j,:}\rangle} \\
=& q\sqrt{l}\sqrt{\sum_{i=1}^l 2p_0 \langle E_{i,:}, E_{i,:}\rangle} \\
=& \sqrt{\frac{2l}{n(n-l)}\|E\|_F^2},
\end{aligned}$$

where we have used

$$\sup_{\|\hat{\mathbf{y}}\|\leq\sqrt{l}} \left\langle \sum_{i=1}^n \sigma_i E_{i,:}, \hat{\mathbf{y}}\right\rangle = \sqrt{l}\left\|\sum_{i=1}^n \sigma_i E_{i,:}\right\|_2$$

in the forth equality, the Jensen inequality in the first inequality, as well as $q\sqrt{Lp_0} = \sqrt{\frac{l}{n(n-l)}}$ in the last equality. Substituting the above bound of $R_{l,n}(\mathcal{H}, p_0)$ into (F.1) and (F.2), the risk bound in (13) is obtained.

Proof of Theorem 5

The proof of Theorem 5 follows immediately from the transductive PAC-Bayesian error bound below (adapted from Corollary 23 of Derbeko et al., 2004):

Theorem 8 *Let the conditions of Theorem 5 hold. Then, for any $\delta \in (0,1)$, with probability at lest $1-\delta$ over random draws of $\mathcal{V}_l$ from $\mathcal{V}$ the following bound holds for any $\mathbf{h} \in \mathcal{H}$*

$$\mathcal{L}_{l,n}(\mathbf{h}) \leq \hat{\mathcal{L}}_{l,n}(\mathbf{h}) + \sqrt{\left(\frac{2\hat{\mathcal{L}}_{l,n}(\mathbf{h})n}{n-l}\right)\frac{ln\frac{1}{P(\mathbf{h})} + ln\frac{l}{\delta} + 7ln(n+1)}{l-1}} + \frac{2\left(ln\frac{1}{P(\mathbf{h})} + ln\frac{l}{\delta} + 7ln(n+1)\right)}{l-1}. \tag{G.1}$$

Since our algorithm is a deterministic algorithm and the selection of the prior distribution $P(\mathbf{h})$ can be made prior to observing the data, we can simply select $P(\mathbf{h}) = 1$ for our algorithm, which leads to the error bound (14) in Theorem 5.

References

R. Agaev and P. Chebotarev. Spanning forests of a digraph and their applications. *Automat. Remote Control*, 62(3):443–466, 2001.

P. Bartlett and S. Mendelson. Rademacher and Gaussian complexities: risk bounds and structural results. *JLMR*, 3:463–482, 2002.

Y. Bengio, O. Delalleau, and N. Le Roux. Label propagation and quadratic criterion. In O. Chapelle, B. Schölkopf, and A. Zien, editors, *Semi-Supervised Learning*, pages 193–216. MIT Press, 2006.

X. Cai, H. Wang, H. Huang, and C. Ding. Simultaneous image classification and annotation via biased random walk on tri-relational graph. In *ECCV*, 2012.

S. Chakrabarti, B. Dom, and P. Indyk. Enhanced hypertext categorization using hyperlinks. In *SIGMOD*, 1998.

O. Chapelle, B. Schölkopf, and A. Zien, editors. *Semi-Supervised Learning*. MIT Press, 2006.

P. Chebotarev and E. Shamis. The matrix-forest theorem and measuring relations in small social groups. *Automat. Remote Control*, 58(9):1505–14, 1997.

P. Chebotarev and E. Shamis. On proximity measures for graph vertices. *Automat. and Remote Control*, 59:1443–1459, 1998.

M. Chen, M. Liu, J. Liu, and X. Tang. Isoperimetric cut on a directed graph. In *CVPR*, 2010.

Fan Chung. Laplacians and the cheeger inequality for directed graphs. *Annals of Combinatorics*, 9 (1):1–19, 2005.

T. Davis. Algorithm 832: Umfpack v4.3—an unsymmetric-pattern multifrontal method. *ACM Trans. Math. Softw.*, 30:196–199, 2004.

Jaydeep De, Huiqi Li, and Li Cheng. Tracing retinal vessel trees by transductive inference. *BMC Bioinformatics*, 15(20), 2014.

J. Demmel, S. Eisenstat, J. Gilbert, X. Li, and J. Liu. A supernodal approach to sparse partial pivoting. *SIAM J. Matr. Anal. App.*, 20:720–755, 1999.

P. Derbeko, R. El-Yaniv, and R. Meir. Explicit learning curves for transduction and application to clustering and compression algorithms. *J. Artif. Intell. Res.*, 22:117–142, 2004.

R. El-Yaniv and D. Pechyony. Transductive Rademacher complexity and its applications. *J. Artif. Intell. Res.*, 35:193–234, 2009.

F. Fouss, K. Francoisse, L. Yen, A. Pirotte, and M. Saerens. An experimental investigation of kernels on graphs for collaborative recommendation and semisupervised classification. *Neural Network*, 31:53–72, 2012.

T. Gartner, Q. Le, S. Burton, A. Smola, and S. Vishwanathan. Large-scale multiclass transduction. In *NIPS*, 2005.

C. Giles, K. Bollacker, and S. Lawrence. Citeseer: an automatic citation indexing system. In *Int. Conf. on Digital Libraries*, 1998.

T. A. Gillette, K. M. Brown, and G. A. Ascoli. The diadem metric: comparing multiple reconstructions of the same neuron. *Neuroinformatics*, 9(2-3):233–245, 2011.

Shantanu Godbole and Sunita Sarawagi. Discriminative methods for multi-labeled classification. In *PAKDD*, pages 22–30. Springer, 2004.

G. Golub and C. Van Loan. *Matrix Computations*. Johns Hopkins University Press, 3rd edition, 1996.

A. Hoover, V. Kouznetsova, and M. Goldbaum. Locating blood vessels in retinal images by piecewise threshold probing of a matched filter response. *IEEE Trans on Med. Imag.*, 19(3):203 –210, 2000.

John G. Kemeny and J. Laurie Snell. *Finite Markov Chains*. Springer, 1976.

J. Leskovec, J. Kleinberg, and C. Faloutsos. Graphs over time: Densification laws, shrinking diameters and possible explanations. In *In KDD*, pages 177–187. ACM Press, 2005.

Q. Lu and L. Getoor. Link-based classification. In *ICML*, 2003.

S. Macskassy and F. Provost. Classification in networked data: A toolkit and a univariate case study. *JMLR*, 8:935–983, 2007.

A. Mantrach, L. Yen, J. Callut, K. Françoisse, M. Shimbo, and M. Saerens. The sum-over-paths covariance kernel: A novel covariance measure between nodes of a directed graph. *IEEE Trans. PAMI*, 32(6):1112–1126, 2010.

Julian J. McAuley and Jure Leskovec. Learning to discover social circles in ego networks. In *NIPS*, pages 548–556, 2012.

A. McCallum, K. Nigam, J. Rennie, and K. Seymore. Automating the construction of internet portals with machine learning. *Inf. Retr.*, 3(2):127–163, 2000.

E. Meijering, M. Jacob, J. Sarria, P. Steiner, H. Hirling, and M. Unser. Design and validation of a tool for neurite tracing and analysis in fluorescence microscopy images. *Cytometry A*, 58(2): 167–76, 2004.

L. Page, S. Brin, R. Motwani, and T. Winograd. The pagerank citation ranking: Bringing order to the web. In *WWW*, 1998.

C. Paige and M. Saunders. Lsqr: An algorithm for sparse linear equations and sparse least squares. *ACM Trans. Math. Softw.*, 8:43–71, 1982.

Y. Saad. *Iterative Methods for Sparse Linear Systems*. SIAM, 2nd edition, 2003.

B. Schölkopf and A. Smola. *Learning with Kernels*. MIT Press, Cambridge, MA, 2002.

P. Sen and L. Getoor. link based classification. Technical report, CS department, Univ of Maryland, 2007. CS-TR-4858.

J. Staal, M. Abramoff, M. Niemeijer, M. Viergever, and B. van Ginneken. Ridge based vessel segmentation in color images of the retina. *IEEE Trans Med. Imag.*, 23(4):501–9, 2004.

A. Subramanya and J. Bilmes. Semi-supervised learning with measure propagation. *JMLR*, 12: 3311–70, 2011.

H. Tong, C. Faloutsos, and J. Pan. Fast random walk with restart and its applications. In *ICDM*, 2006.

E. Turetken, C. Becker, P. Glowacki, F. Benmansour, and P. Fua. Detecting irregular curvilinear structures in gray scale and color imagery using multi-directional oriented flux. In *ICCV*, 2013a.

E. Turetken, F. Benmansour, B. Andres, H. Pfister, and P. Fua. Reconstructing loopy curvilinear structures using integer programming. In *CVPR*, 2013b.

H. Wang, C. Ding, and H. Huang. Directed graph learning via high-order co-linkage analysis. In *ECML*, 2010.

J. Wang, T. Jebara, and S. Chang. Semi-supervised learning using greedy max-cut. *J. Mach. Learn. Res.*, 14(1):771–800, 2013.

X. Wu, Z. Li, A. So, J. Wright, and S. Chang. Learning with partially absorbing random walks. In *NIPS*, 2012.

D. Zhou, O. Bousquet, T. Lal, J. Weston, and B. Scholkopf. Learning with local and global consistency. In *NIPS*, 2004.

D. Zhou, J. Huang, and B. Schölkopf. Learning from labeled and unlabeled data on a directed graph. In *ICML*, 2005.

X. Zhu and A. Goldberg. *Introduction to Semi-Supervised Learning*. Morgan & Claypool, 2009.

X. Zhu, Z. Ghahramani, and J. Lafferty. Semi-supervised learning using gaussian fields and harmonic functions. In *ICML*, 2003.

Xiaojin Zhu, Andrew Goldberg, Jurgen Van, and Gael David Andrzejewski. Improving diversity in ranking using absorbing random walks. In *HLT-NAACL*, 2007.